Single Stage Transformer Isolated High Frequency AC Link Inverters without the Problem of Leakage Energy Commutation

A DISSERTATION
SUBMITTED TO THE FACULTY OF THE GRADUATE SCHOOL
OF THE UNIVERSITY OF MINNESOTA
BY

Sesha Sai Srikant Sarma Gandikota

IN PARTIAL FULFILLMENT OF THE REQUIREMENTS
FOR THE DEGREE OF
DOCTOR OF PHILOSOPHY

Ned Mohan

November, 2016

Acknowledgements

This thesis would not have been possible without the help and guidance of several people over the past few years. I express my sincerest gratitude to my advisor, Ned Mohan, for inspiring me and encouraging me. I was fortunate to be surrounded by wonderful colleagues and friends during my time at the University of Minnesota. Ashish, Kartik and Shrivatsal deserve a special mention for being such amazing roommates and even better friends. Saurabh, Eric, Rohit, Shabari and Kaushik have been extremely helpful in several ways and I have definitely benefited from their advice. I should also mention Suvankar, Siddharth, Santhosh, Ruben and Varsha for making my time at the lab so memorable.

I can never thank my parents enough for their support and giving me the freedom to follow my dreams. This thesis would also not have been possible without the love and affection of my wonderful brother Rohit and my fiancee Aditi who have always been there for me.

Dedication

To my parents and brother.

Abstract

High frequency AC link based converters offer several desirable features such as improved power density, galvanic isolation and improved reliability due to the absence of an electrolytic capacitor. The power conversion happens through a high frequency link which operates in the tens of kilohertz range and consequently, the size of magnetic components is reduced. An AC or DC voltage source is 'chopped' by a converter to generate the high frequency voltage which is applied to a transformer that can be used to provide the necessary voltage transformation. On the secondary winding of the transformer, the high frequency voltage is directly converted to synthesize the desired output voltages which are at a much lower frequency than the AC link. Unlike DC bus based topologies, there is no need for a power stage to first rectify the AC link before generating the output voltage.

Despite several advantages, transformer isolated single stage power conversion requires the use of a voltage clamping circuit across the AC link for its operation due to the presence of transformer leakage inductance. When high frequency AC link voltage is directly used to synthesize the output voltages, the link currents exhibit sudden polarity reversals. Due to the presence of leakage inductance, which is unavoidable in transformers, large voltage spikes result during the current reversal instants and necessitate the use of additional circuitry to limit such overvoltages. This limitation, which is termed the problem of leakage energy commutation, needs to be overcome to prevent the link voltage from exceeding the breakdown voltages of the switches, damaging winding insulation or causing unwanted distortion in the output voltage.

This thesis proposes two implementations of transformer isolated high frequency link inverters that overcome the problem of leakage energy commutation. The inverters consist of a H-Bridge to generate the high frequency voltage from a DC voltage source and a cycloconverter to generate the output voltages. In the first implementation, a parallel LC tank is proposed to be connected across the secondary winding of the transformer to ensure the current through the leakage inductance does not have sudden reversals. The high frequency transformer along with the LC tank results in a sinusoidal voltage which is applied across the cycloconverter. A discrete space vector modulation

technique is used to synthesize three phase output voltages and any change of switch states in the cycloconverter is restricted to the zero crossing regions to avoid switching losses. The second approach proposes using an additional leg across the cycloconverter to induce a resonant current transition when the current flowing through the transformer has to reverse its polarity. The additional leg, comprising of a bidirectional switch and a small capacitor, is only used for a short interval during which it resonates with the leakage inductance. The operation and analysis of the proposed ideas are discussed in this thesis and have been validated through computer simulations. A hardware prototype was constructed to demonstrate the operation of a high frequency link inverter using the LC tank and the results are found to be in agreement.

Contents

List of Tables

List of Figures

Chapter 1

Introduction

The effects of global warming and climate change have strongly influenced the ways in which electric energy is being generated and consumed [1]. Rising global temperatures have forced us to look for sustainable and cleaner ways to supply the ever increasing energy demands of the world. At the same time, there has been increasing emphasis to develop highly efficient products that minimize losses. As a result, every stage of the power system, starting from the source of generation to end use has witnessed the proliferation of state of the art power electronic technologies. Even the automobile industry, which has traditionally used fossil fuels to power internal combustion engines, is seeing a rising interest in electric vehicles.

Power electronics has played a major role in transforming the electric power system [2]. Today, several countries have plans to install large scale solar farms and reduce their dependence on coal fired power plants. Solar inverters serve as the connection point to the electric grid and are an essential component of such systems. Advances in power semiconductors over the years have made it possible to design inverters that run cooler and consequently improve the lifetime and reliability of solar installations. The development of smaller string inverters has made rooftop solar panels an attractive option at a residential level. The high switching frequency made possible in these string inverters results in a compact form factor and easy installation.

Wind energy has similarly seen improved adoption rates. Several power electronic architectures which facilitate the use of high frequency transformers in the nacelle of the wind turbine have helped reduce the size of long cables that carry power to the

base of the wind turbine. Large scale offshore wind farms are now feasible due to the availability of HVDC transmission technology that offers several advantages. Batteries and flywheels serve as buffers to compensate for the variability in these renewable sources by storing energy and making it available when needed. This kind of bidirectional power flow can be easily achieved using power converters that can be controlled to precisely meet the active and reactive power requirements. Electric motors find widespread use in a variety of industries and are a major consumer of electric power. The efficiency of such motors is enhanced by the use of variable frequency drives which can generate flexible voltage outputs. By using an active front end interface comprising of controlled switches, it is possible to regulate the injection of unwanted harmonics into the grid. Electric motors have also been proposed for use in ships, aircraft and electric cars.

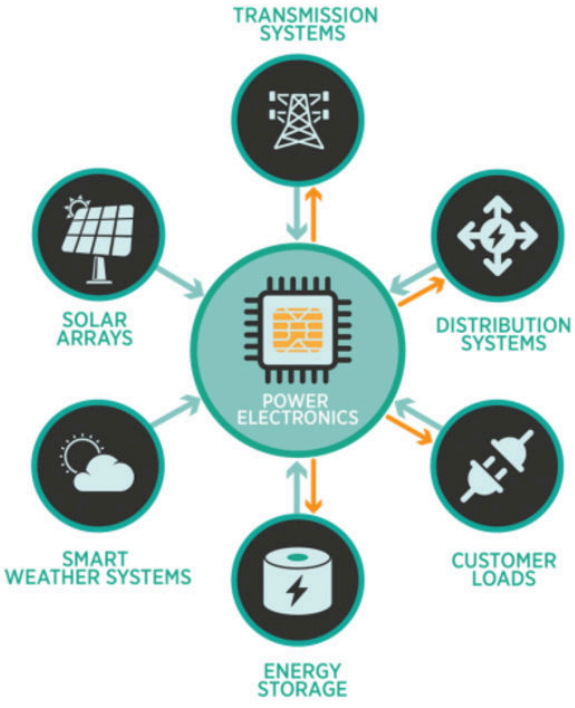

Figure 1.1: The role of power electronics [3]

All these examples demonstrate the versatile roles played by power electronics in

helping transition to cleaner ways of generating and consuming electric power. High efficiency, adaptability and improved power density are some of the salient characteristics that have enabled power electronic converters to be so effective. All these benefits are easily combined in high frequency AC link power inverters which are described in this thesis. As the name suggests, these converters use a high frequency AC link instead of the commonly used DC link. The AC link makes it possible to employ a transformer to achieve galvanic isolation and voltage transformation while the high frequency reduces the size of such magnetic components. The reliability of the converters is improved by avoiding the use of electrolytic capacitors and using single stage conversion. However, the leakage inductance of the high frequency transformer can cause large over voltages in the AC link when single stage conversion is used. This thesis presents techniques to overcome the problem of leakage energy commutation and describes them in detail with the goal of making three phase high frequency AC link inverters practically feasible.

1.1 DC-AC power conversion

Voltage source inverters(VSIs) are a very well researched topic and find extensive use in several single and three phase applications. A DC voltage with a constant magnitude is switched to generate AC voltage at the desired frequency and magnitude. Power semiconductors such as IGBTs or MOSFETs are used to switch the DC voltage according to a switching pattern given by a modulating signal. A variable AC voltage is generated from a fixed DC voltage by controlling the width of the voltage pulses and as such, this technique is called pulse width modulation(PWM).

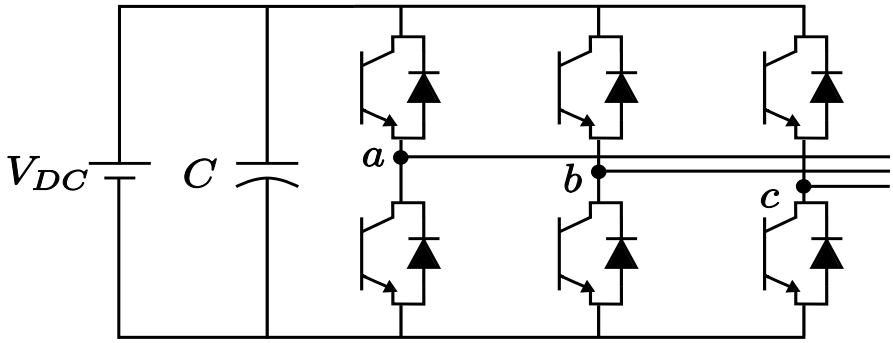

Figure 1.2: Voltage source inverter

The power converter consists of three legs each comprised of a top and bottom switch as shown in Fig. 1.2. The DC side consists of a filter capacitor, C, and the DC power source denoted as V_{DC}. The top and bottom switches in a phase leg are alternately turned on to generate a switching output voltage. The rate at which they are switched is called the switching frequency. The switching voltage consists of the fundamental voltage at the desired frequency and several voltage harmonics which are multiples of the switching frequency.

The efficiency of a voltage source inverter is strongly influenced by the switching and conduction losses of the switches. The switching losses increase with the switching frequency and can be the major source of power losses necessitating the use of large heat sinks. Using SiC based switches can help reduce these losses to a certain extent but it still results in a large $\frac{dv}{dt}$ that can cause EMI issues and problematic bearing currents when used in electric drive applications [4]. The reliability of VSIs is influenced by the use of electrolytic capacitors in the DC bus. The lifetime of electrolytic capacitors is considerably lower than a film capacitor and reduces the lifetime of the overall inverter [5].

Several methods were proposed to overcome these shortcomings in voltage source inverters. By introducing additional circuit elements that introduce resonant intervals, periods of zero voltage or zero current can be obtained to facilitate zero switching losses [6] and also mitigate electromagnetic emissions. These circuits can be classified according to the location where resonance occurs [7] i.e either at the load end or at the bus. Load resonant converters have the load connected in series or parallel across a resonant network and result in Zero Voltage Switching/Zero Current Switching of the devices. The resonant frequency of the passive network is slightly larger than the output frequency and the resonating voltage/current is used to achieve soft switching. However, the operation of this converter is dependent on the load and they are more suited for applications where the load is fixed. The resonant pole inverter(RPI) restricts the resonant intervals to a short time and is only activated when the switches have to change state. However, the inductor current has a high peak to average ratio and can result in a large sized inductor and increased switch ratings. Moreover, in these type of soft switching converters, the resonant inductor is in the path of the load current and can result in significant conduction losses. Alternately, an auxiliary resonant commutated

pole inverter(ARCPI) [8] has been proposed in which the resonant inductor is not in the path of the load current. The resonant inductor is connected in series with a controlled switch which when turned on initiates a resonance with a capacitor across the switch and results in a ZVS transition.

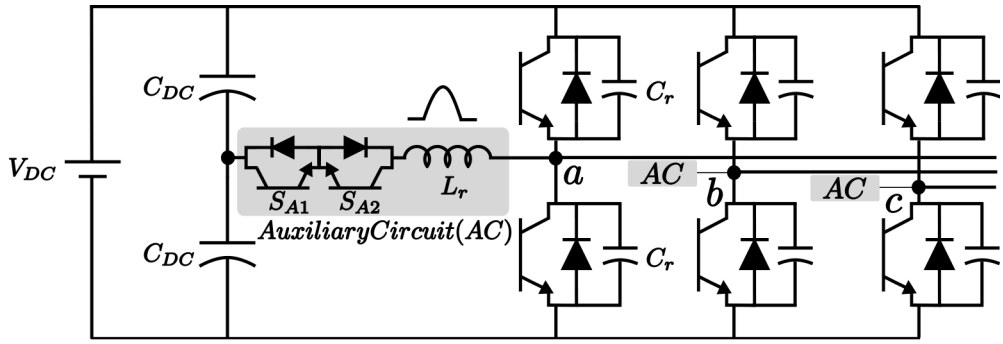

Figure 1.3: Auxiliary Resonant Commutated Pole inverter

The Resonant DC link inverter was first proposed by [9] and operates by introducing resonance on the DC bus. This is obtained by connecting an inductor in the DC bus and resonating it with a capacitor connected across the three phase bridge. A phase leg is shorted causing the current in the inductor to build up to a predetermined value. At the end of this linear current buildup stage, a resonance occurs between the DC bus inductance and capacitance and the DC bus voltage swings to zero voltage after a short time. By restricting the change of inverter switch states to these regions of zero voltage, soft switching is achieved. Since all the switches have to change state at the same time, the output is synthesized using a discrete pulse modulation scheme. Variations of the resonant DC link exist such as the actively clamped DC link scheme [10] or the quasi resonant DC-link [11] schemes to reduce the switch stresses and improve the PWM performance.

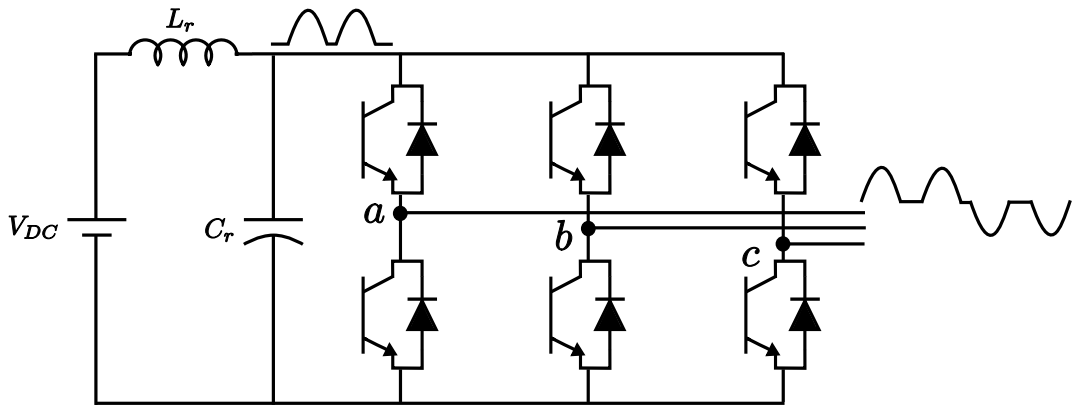

Figure 1.4: Resonant DC Link inverter

1.2 Transformer isolated inverter configurations

The previous section has described the traditionally used VSI's and improvements that alleviate the problem of switching losses and large $\frac{dv}{dt}$. Many times, there is a need to connect a transformer to account for large variations between input and output voltages. Transformers provide a simple way of stepping up/down the voltage levels and also provide galvanic isolation between two stages. Having a transformer isolated inverter also helps provides safety and can prevent faults from propagating to other parts of the system. The most direct way of achieving galvanic isolation is by connecting a low frequency transformer at the line frequency output terminals of the inverter but the resulting transformer is large and heavy. It is well known that the physical size of the transformer is inversely proportional to the frequency of voltage that is applied across it. This means that a transformer operating at higher frequencies can be smaller as compared to a transformer operating at 60Hz.

Hence, when designing transformer isolated inverters, it is advantageous to use two stages of power conversion. The first stage consists of a DC/DC stage where high frequency operation is possible and hence provides the opportunity to embed a high frequency transformer. The second stage would then generate the desired 60Hz voltages using the DC voltage output of the first stage. The dual active bridge(DAB) converter or the LLC converter are very commonly used to construct the high frequency isolated DC-DC stage.

A solid state transformer using the DAB topology as the DC-DC isolated stage is described in [12]. The use of active switches to construct the full bridges in a DAB allows bidirectional power flow and the direction of power flow is controlled by adjusting the phase shift between the voltages generated by the full bridges. Several schemes have been proposed that deal with extending the range of soft switching in DAB converters and achieving better low load efficiencies [13].

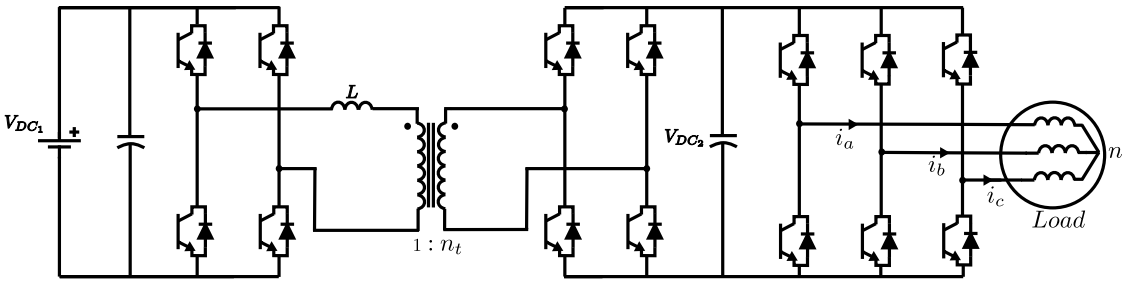

Figure 1.5: Dual active bridge based isolated DC-AC implementation

The LLC converter looks similar in construction to a series resonant converter but utilizes the magnetizing inductance of the transformer to achieve different gain characteristics [14]. ZVS turn on is possible for the switches while the turn off current is lower than the peak tank currents. The secondary diodes are turned off at zero current thereby limiting the reverse recovery losses. The power can be varied by adjusting the frequency of the voltage applied by the primary bridge. The LLC converter is also capable of bidirectional power flow when active switches are used on the secondary side of the transformer [15].

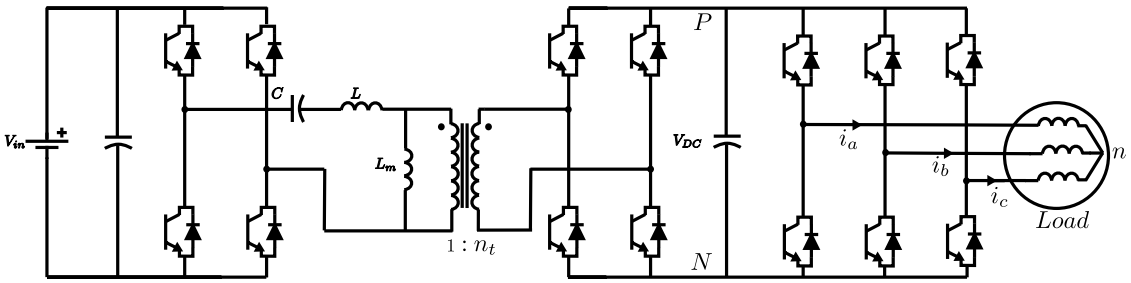

Figure 1.6: LLC converter based isolated DC-AC implementation

While both the LLC and DAB converters are capable of soft switching, the resulting power conversion from DC to 60Hz AC takes place in two stages. Due to this, the overall efficiency of the converter is reduced. Moreover, while this scheme helps use a compact high frequency transformer, it still uses electrolytic capacitors to establish the intermediate DC bus and this is detrimental to the reliability of the system.

1.3 High Frequency AC Link Systems

High frequency AC link converters have emerged as an attractive alternative to traditional DC bus systems. Instead of a stable DC bus, the power transfer happens through a link with a high frequency alternating voltage/current. Topologies using a high frequency voltage link are more common where the DC voltage is chopped, usually by using a H-bridge(full bridge) inverter, to generate the high frequency waveform. Zero crossings in the link voltage exist and can be utilized to eliminate switching losses. Another desirable feature of high frequency AC link converters is the ability to connect a high frequency transformer to achieve electrical isolation. The transformer can provide a step up/step down of the voltage with a suitable turns ratio. Further, the high frequency link enables the use of small valued reactive components and a compact transformer.

Some of the earliest papers describing a high frequency power transfer scheme were proposed by McMurray [16,17] and by [18]. Subsequently, power transfer using twin resonant high frequency links was proposed by [19] while [20] compared resonant inverters for PV to utility interface. Subsequently, [21, 22] reported a 20kHz single phase voltage link power distribution scheme which uses a pulse density modulation(PDM) scheme. A high frequency link implementation for uninterruptible power supplies was described in [23] and employs a PWM scheme. It is clear that the merits of high frequency link schemes were well established at an early stage. A review of recent publications reveals a growing interest in AC link based power conversion schemes [24–28].

The use of a high frequency AC link means that large and unreliable electrolytic capacitors can be avoided and can be replaced by a longer lifetime film capacitor. It has been shown that although electrolytic capacitors are an economical option, they have poor lifetime and thus affect the reliability of the overall system [5, 29]. Replacing

the electrolytic capacitors with film capacitors has been shown by [30] to improve the weight, size and lifetime. Similarly, the results reported by [31] show a considerable increase in the power density of an inverter when using a high-current film capacitor.

Despite the use of different modulation schemes and construction, several advantages of high frequency AC link converters become apparent such as

- higher efficiencies due to soft switching
- improved reliability by avoiding electrolytic capacitors
- improved power density due to small sized magnetics and
- electrical isolation and voltage step up/down

1.4 Problem of Leakage energy commutation

While single stage transformer isolated converters offer several attractive features, problems arise due to the non ideal nature of the high frequency transformer. A transformer provides isolation between two electrical circuits and the power transfer happens through a magnetic core as shown in Fig. 1.7. In an ideal transformer, the flux generated by one winding will completely link the second winding. However, in practice, some portion of the flux does not link the other winding and gives rise to a leakage flux. Now, this leakage flux can be represented as an inductance in the equivalent model of a transformer and is termed the leakage inductance. In a practical two winding transformer, there is a finite leakage inductance associated with the primary winding and the secondary winding as shown in Fig. 1.7.

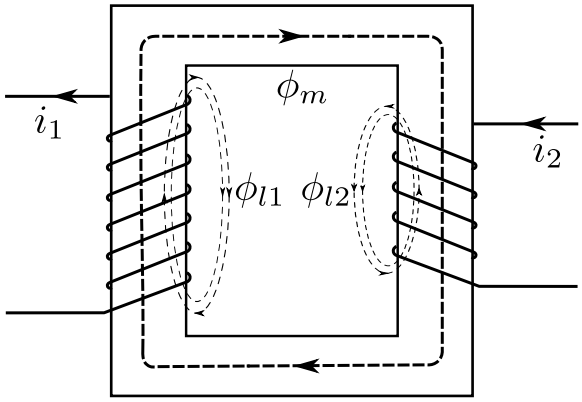

Figure 1.7: Leakage flux in a transformer

Leakage inductance plays a critical part in power electronic designs that use transformers. Depending on the kind of topology, leakage inductance can be desirable or problematic. For instance, a dual active bridge topology [32] uses the leakage inductance to transfer power and the transformer is purposefully designed for a particular value of leakage inductance. The ZVS phase shift full bridge converter [33] uses the leakage inductance for soft switching the devices.

In a single stage power conversion scheme, the currents which flow through the transformer are a function of the load current and the switching state of the cycloconverter. To optimize the switching loss in the cycloconverter, the switch states are only changed near the zero crossings. Assume that a DC current I is flowing at the output and a DC voltage is being synthesized from a transformer isolated high frequency link. Depending on the output DC voltage desired, the duty ratio is compared with a carrier signal and the link polarity to obtain the switching signals. As a result, the current through the transformer has a square waveshape as shown in Fig. 1.9 and has regions with a high rate of change ($\frac{dI}{dt}$). When such a current flows through the transformer and its leakage inductance, it results in a large voltage spike at every transition as described by 1.1

$$v = L_{lkg}\frac{di}{dt} \tag{1.1}$$

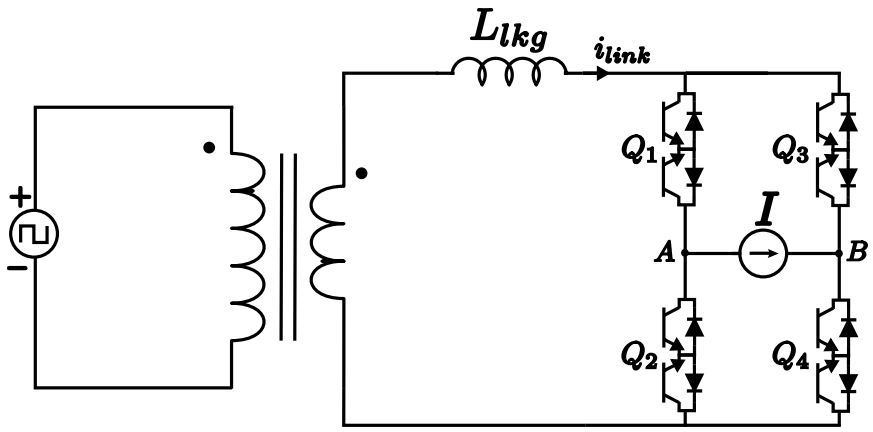

Figure 1.8: Problem of leakage commutation

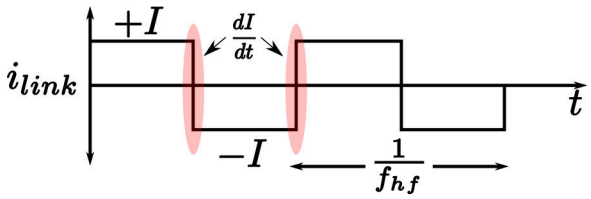

Figure 1.9: Shape of current i_{link}

The magnitude of the voltage spike is directly dependent on the value of L_{lkg} and can damage the transformer insulation, exceed the maximum voltage rating of the switches and result in distortion of the output voltage. The problem of overvoltages appearing across the transformer windings caused due to the leakage inductance was reported in [34–37]. A simple way of minimizing the effect of the voltage spike is to connect a voltage clamping circuit across the AC link. A single phase clamp is shown in Fig. 1.10 and is realized by connecting a capacitor C_{clamp} and resistor R_{clamp} at the output of a diode bridge. The voltage of C_{clamp} is maintained higher than the normal voltage range of the AC link. Whenever the voltage across the link starts increasing due to sudden current reversal through the leakage inductance, the diode bridge is activated and the voltage across the link is limited to the clamp voltage. Consequently, this clamp voltage is applied across the output terminal and leads to unwanted distortion. The R_{clamp} is sized to maintain the voltage across C_{clamp} and is used to dissipate energy due to leakage commutation. It can be seen that although this method limits the voltage spike,

it is not a very efficient method of accomplishing it.

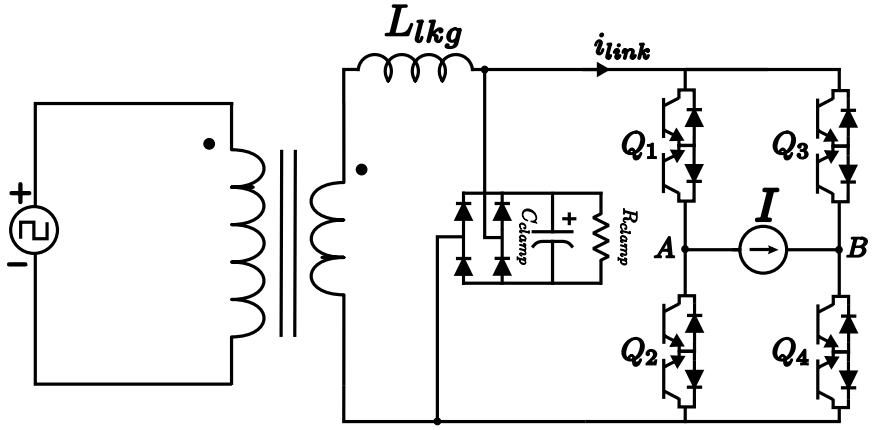

Figure 1.10: Diode clamp to limit voltage spike

A source based commutation technique has been explained in [35] to overcome this problem. As the name suggests, the voltage of the source is applied with the required polarity to ensure a natural commutation occurs and current through the leakage inductance is linearly reversed. However, this could lead to additional switching on the source side converter as the correct link polarity has to be applied every time the link current has to change direction. Another approach which proposes the use of a resonant tank to ensure that the link current is sinusoidal and hence ensuring that there is no problem of leakage energy is described in [38, 39].This method avoids the need for any source side switching or dissipative clamp circuits. However, it requires the use of reactive components in the link which need to handle large currents due to the resonant operation. Alternately, a multi-level asymmetrical transformer with interleaved windings was used to minimize the leakage inductance and reduce the problem of leakage energy commutation in [40].

1.5 Applications

The use of high frequency AC link inverters for various applications are discussed in this section. The features and characteristics of each implementation areas are also

presented. High frequency, transformer isolated inverters find widespread use in interfacing renewable sources such as photovoltaic panels [41], fuel cells [42] and also other applications like UPS systems [37].

1.5.1 PV to grid interface

A PV panel produces a DC voltage that needs to be converted to AC voltage at the grid frequency. The conversion is performed in two stages and in the first stage, a DC-DC converter is used to boost the output voltage of a PV panel or string of PV panels. Once the required DC bus voltage is established, an inverter switches this bus voltage to generate a pulse width modulated waveform that is interfaced to the grid. Electrical isolation is needed to ensure safety due to the problem of leakage currents. The transformer can be connected on the low frequency side at grid frequency or a high frequency transformer that is usually a part of the DC-DC stage. It is advantageous to connect the transformer on the high frequency side as the size of the transformer is greatly reduced as shown in Fig. 1.11.

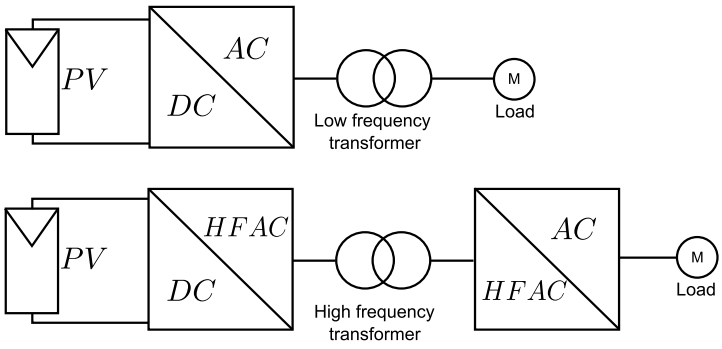

Figure 1.11: Inverter configurations with transformer isolation

A high frequency AC link inverter can also be used to interface a PV source with the grid and take advantage of high frequency transformer isolation. The benefit of a single stage approach is that it eliminates the need for electrolytic capacitor which is needed in a two stage approach. Moreover, the overall efficiency reduces when multiple power conversion stages are used. The design and operation of a high frequency AC link inverter is presented in [28, 43, 44]

1.5.2 Battery Storage and UPS Applications

The variable nature of PV and wind energy sources necessitates the use of energy storage systems to ensure a reliable power supply. Battery storage systems and uninterruptible power systems(UPSs) have been proposed along with flywheels, compressed air storage systems etc. These systems should have the capability to store energy when the power generation exceeds demand and subsequently be able to supply the stored energy. The power converter used for these applications should therefore be capable of bidirectional power flow and high frequency AC link based UPS configurations have been reported in [45, 46].

1.5.3 Electric Drives

The use of high frequency AC link converters for electric drives applications has been demonstrated in [47–49]. The ability to soft switch means that a high control bandwidth can be achieved and output filter size can be reduced.

1.6 Contributions

The goal of this dissertation was to investigate new techniques to overcome the problem of leakage commutation in single stage high frequency inverters. Specifically, the investigation was focused on realizing a high frequency AC link inverter which does not require the use of additional clamp circuits. The results discussed in this thesis are an extension of the work reported in [50], which proposed using the leakage inductance of the transformer in conjunction with an additional capacitor to realize sinusoidal currents through the transformer. This thesis proposes two alternative approaches to avoid fast changing currents through the transformer. The major contributions can be summarized as follows :

1. The use of a parallel LC tank connected across the secondary of the transformer is shown to help avoid the problem of leakage energy commutation and avoids the need for additional voltage clamping circuits in the AC link.

2. A space vector modulation technique was developed to generate balanced three phase voltages from a sinusoidal high frequency link.

3. The modulation technique developed has the advantage of restricting any change of cycloconverter switch states to the zero crossing regions and eliminates the switching losses in the three phase cycloconverter. This allows the use of higher link frequencies and improves the efficiency.

4. The operation of an open end drive with a transformer isolated high frequency AC link is proposed and does not have large $\frac{dv}{dt}$ at the motor terminals.

5. A partial resonant commutation technique is described which helps avoid the problem of leakage energy commutation.

1.7 Organization of this thesis

This chapter was aimed at explaining why single stage high frequency AC link converters are attractive and the problem of leakage energy commutation. The idea of using a parallel LC tank across the cycloconverter to avoid the problem of leakage energy commutation is described in Chapter 2. The associated space vector modulation technique is explained and the results are analyzed. The idea explained in Chapter 2 is extended to an open end drive in Chapter 3. A new commutation technique that uses an additional leg to avoid the problem of leakage energy commutation is presented in Chapter 4. A brief summary of the work and possible areas of future research are reported in Chapter 5.

Chapter 2

High Frequency AC Link Inverter using a Parallel LC Tank

2.1 Introduction

This chapter describes a cycloconverter based three phase inverter which uses a high frequency transformer isolated AC link comprising of a parallel resonant tank across the secondary winding of the transformer[1] . Cycloconverter based power converters have been reported by [36,37]. In these implementations, a H-bridge is used to generate high frequency AC voltage from the DC source which is then applied across the primary winding of a high frequency transformer. The transformed voltage across the secondary winding is directly converted to the desired lower frequency voltage by a cycloconverter bridge. This single stage power conversion is different from two stage topologies, which first rectify the high frequency AC voltage to DC and then invert it to generate the output voltages.

However, when single stage conversion is used, the leakage inductance of the high frequency transformer results in large voltage spikes when the current flowing through it is abruptly changed due to the switching of the cycloconverter. This problem is inevitably present as leakage inductance is unavoidable in a transformer winding. Reference [52] uses a clamp circuit to limit this voltage rise. However, use of a clamp circuit

[1] Parts of this chapter are taken from [51]

is a lossy solution. A non-resonant inverter with integral pulse modulation technique leading to a quasi soft switching in the cycloconverter was proposed in [47]. Here too a snubber circuit is used to absorb the energy trapped in the leakage inductance of the transformer. In [48], an inverter implementation was proposed that facilitates the complete recovery of the leakage energy.

As explained in reference [53], the problem of leakage energy commutation can be avoided by ensuring that the current through the leakage inductance of the transformer is sinusoidal. Having sinusoidal current through the transformer also reduces the winding losses and can lead to a more compact transformer design as explained in [54]. This helps avoid the problem of leakage energy commutation. The operation of this converter and various results are presented.

2.2 Circuit Description

The proposed three phase inverter using a high frequency AC link is shown in Fig. 3.2. A H-bridge comprising of switches S_a through S_d is used to convert the DC voltage to a high frequency alternating voltage denoted as v_{switch} that is fed to the transformer primary winding. The L_{lkg_p} and L_{lkg_s} represent the leakage inductances of the transformer windings and the voltage across the secondary winding is denoted as v_{hf}. The cycloconverter connected to the secondary winding of the transformer comprising of the switches S_{AP} through S_{CN} is used to synthesize three phase voltages of adjustable magnitude and frequency from the high frequency link voltage. Switches with bidirectional voltage blocking ability need to be used in the cycloconverter in order to be able to block the alternating link voltage. A parallel combination of an inductor,L_p and capacitor, C_p is connected across the secondary terminals of the transformer.

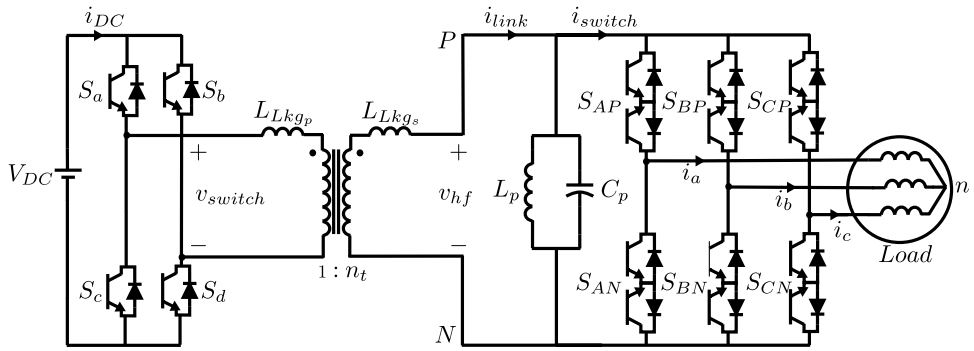

Figure 2.1: Inverter Topology

The voltage generated by the H-bridge is called v_{switch} and the current generated by the cycloconverter is called i_{switch}. A three phase load supplied by the cycloconverter and the phase currents are shown in Fig. 3.2. The load can be either a motor or a three phase grid and the power flow can be in either direction.

2.3 Principle of Operation

The problem posed by the leakage inductance arises due to the fact that switching the cycloconverter results in an abrupt change of current through the L_{lkg}. Sudden changes in the current through an inductor will result in a high voltage across the link which could potentially damage the switches or breakdown the winding insulation. To avoid these problems, the parallel resonant tank is used to ensure that the current flowing through the transformer is sinusoidal and thus avoid a large $\frac{di_{link}}{dt}$.

The impedance of the tank as a function of the frequency is given by 2.1 and is plotted in Fig. 2.2. It can be observed from the impedance diagram of the resonant tank that it presents a very high impedance at its resonant frequency and a low impedance to all the other frequency components. This means that the resonant tank acts as a low impedance path to the high frequency components of current i_{switch} whose shape depends on the cycloconverter switch state and the output currents.

$$Z(\omega) = \frac{\omega L}{1 - (\frac{\omega}{\omega_{hf}})^2} \tag{2.1}$$

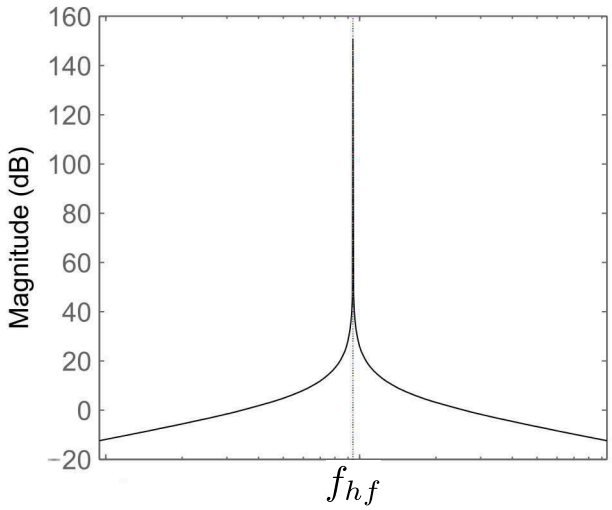

Figure 2.2: Impedance of the tank as a function of frequency

The AC link frequency is chosen to be the same as the resonant frequency f_{hf}. This resonant frequency depends on the values of L_p and C_p and is given by 2.2.

$$f_{hf} = \frac{1}{2\pi\sqrt{L_p C_p}} \tag{2.2}$$

2.3.1 Modulation of H-bridge

The input H-bridge is switched to apply a high frequency switching voltage across the primary winding of the transformer with a fundamental frequency of f_{hf}. Turning on the switches S_a and S_d results in the application of the non-zero levels $v_{switch} = +V_{DC}$ to the primary winding while turning on switches S_b and S_c results in the application of $V_{switch} = -V_{DC}$. Switching alternatively between these two switching states would lead to the generation of a high frequency square wave voltage at the transformer primary winding. The harmonic analysis of such a square wave voltage reveals the existence of odd harmonics with considerable magnitude. Given the low impedance of the tank at frequencies other than f_{hf}, these harmonics in the voltage generated by the H-bridge will result in additional currents at these harmonic frequencies flowing into the tank. This leads to unwanted circulating currents and over-sizing of the transformer and additional

power losses within it.

This unwanted circulating current can be prevented if the H-bridge is switched such that the switching harmonics are very far from the fundamental frequency. The impedance offered by the leakage inductance linearly increases with the frequency and suppress circulating currents. The Selective Harmonic Elimination techniques presented in reference [55] can be used to generate the required v_{switch} while eliminating certain low order harmonic

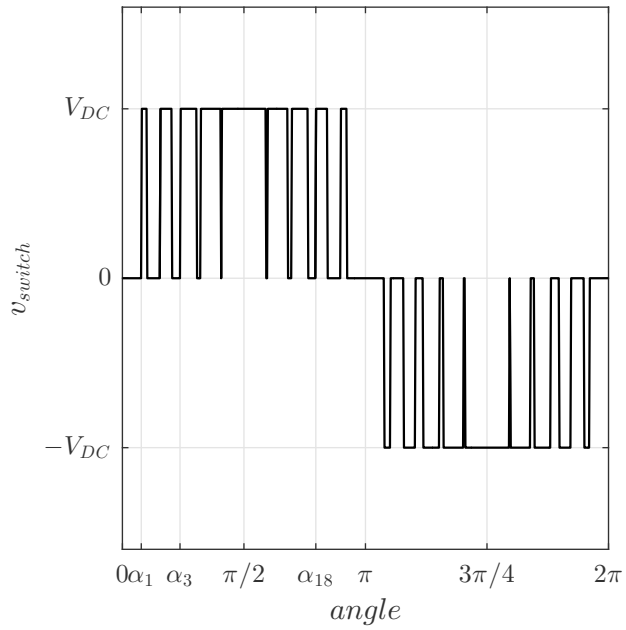

Figure 2.3: H Bridge Output

By switching the input H-bridge at specific pre-calculated instants of time within one fundamental cycle of f_{hf}, higher order harmonics in the voltage are eliminated. The more the number of harmonics to be eliminated, the higher will be the number of switching instants. The SLL technique presented in [55] has been used and the maximum peak voltage of the link voltage with this technique is equal to V_{DC} i.e the modulation index of the H-Bridge is $m_{vH} = 1$. The modulation index is defined as the ratio of peak value of the fundamental frequency of v_{switch} to the magnitude of V_{DC} as defined in 2.3. In this programmed PWM scheme, switching instants leading to elimination of certain harmonic frequencies are computed by solving a set of non linear equations. In

the following analysis, the H-bridge is switched so as to eliminate the 3,5,7,9,11,13,15 and 17th harmonics from the voltage generated by it. Fig. 2.3 shows the shape of the voltage generated by the H-bridge.

$$m_{vH} = \frac{v_{switch_1}}{V_{DC}} \tag{2.3}$$

2.3.2 Modulation of the cycloconverter

The effect of the transformer leakage inductance and the tank on the switching voltage can be analyzed by considering the voltage transfer function of the link. The transformer is assumed to have a large magnetizing inductance which can be omitted and a lumped model of the leakage inductance is used. A finite winding resistance of the transformer is assumed as R_w and the series resistance of the inductor L_p is represented as R_p as shown in Fig. 2.4. The voltage transfer function can be obtained from this circuit and is shown in 2.4.

$$G_v(s) = \frac{V_{hf}(s)}{V_{switch}(s)} = \frac{sL_p + R_p}{\mathrm{s}^3 L_p L_{lkg} C_p + s^2 (L_{lkg} R_p + L_p R_w) C_p + s (L_{lkg} + L_p + C_p R_p R_w) + R_p + R_w} \tag{2.4}$$

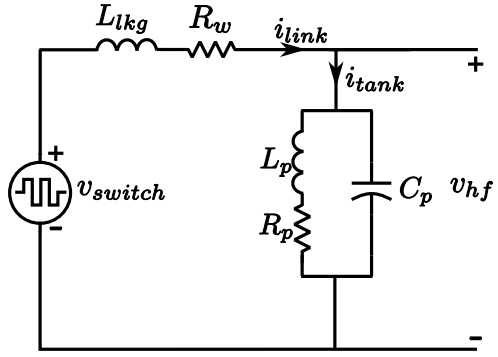

Figure 2.4: Equivalent circuit of the AC link

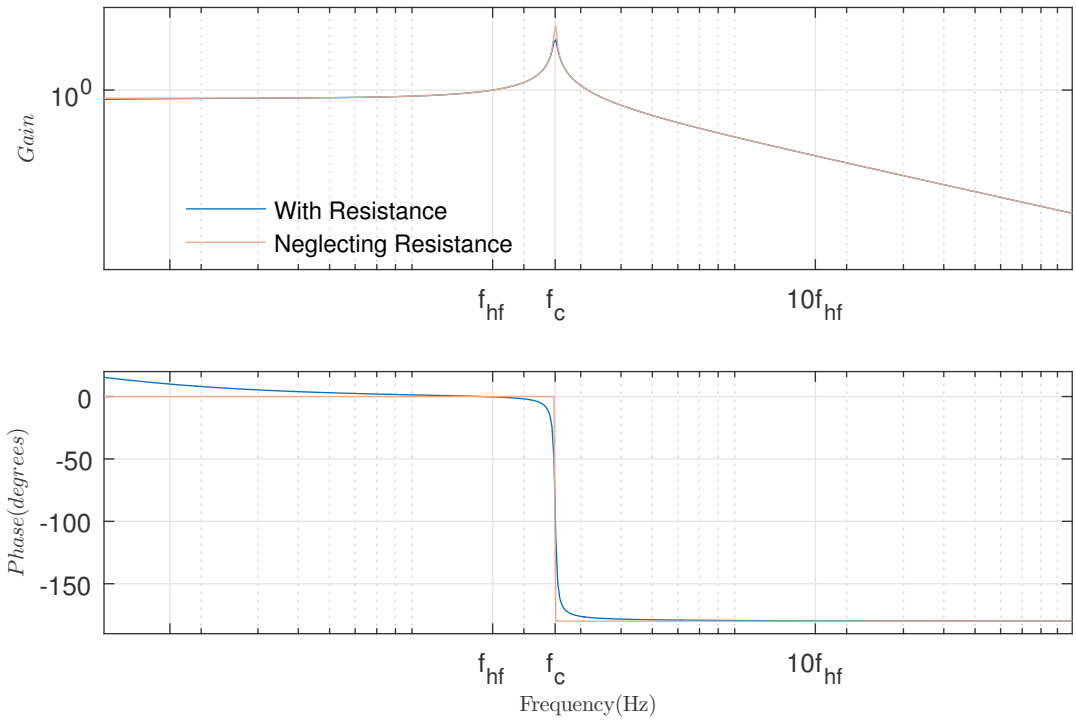

Figure 2.5: Voltage transfer function

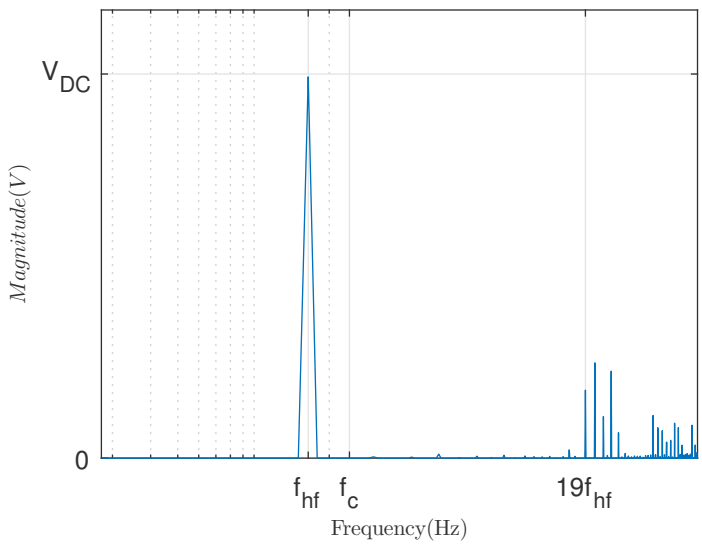

Figure 2.6: Harmonic spectrum of v_{switch}

The Bode plot of the voltage transfer function shows that the gain of the tank at the link frequency, f_{hf}, is unity and the peak value occurs at the frequency f_c. By neglecting the winding resistances, the location of the peak can be calculated as 2.5. The effect of the winding resistances is to reduce the peak value of the transfer function as shown. Beyond f_c, the gain of the voltage transfer function continues to decrease thus attenuating any harmonics of v_{switch} that occur in this region. The harmonic spectrum of the voltage v_{switch} is shown in Fig. 2.6 and the first harmonic occurs at the frequency $19f_{hf}$ due to the SHE modulation. Thus, the harmonics in v_{switch} are attenuated and the resulting voltage v_{hf} across the secondary winding is sinusoidal at the link frequency as shown in Fig. 2.7.

$$f_c = \frac{1}{2\pi\sqrt{\frac{L_{lkg}L_p}{L_{lkg}+L_p}C_p}} \tag{2.5}$$

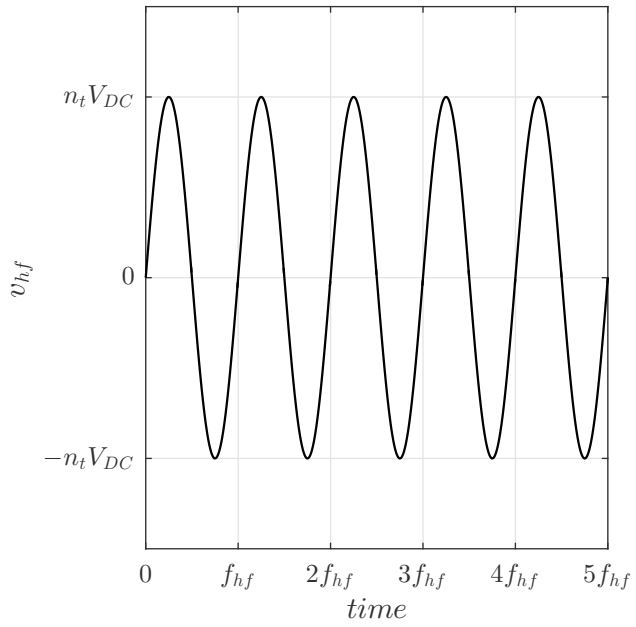

Figure 2.7: Plot of v_{hf}

The cycloconverter now has the task of synthesizing three phase voltages of adjustable magnitude and frequency from v_{hf} which has a sinusoidal shape. The modulation strategy is designed to restrict device switching to the zero crossings of the link

voltage thereby eliminating switching losses over the entire operating range.

The space vector modulation(SVM) technique has been extensively used in conventional voltage source inverters. In this technique, the desired output space vector $\overrightarrow{V_s}$ is synthesized by applying a suitable combination of active voltage vectors and zero voltage vectors. The spacevector is defined as 2.6. These vectors and the associated switch combinations are illustrated in the voltage space vector diagram of Fig. 2.8. A switch state [100] indicates that the switches S_{AP}, S_{BN} and S_{CN} are turned on and so on. For example, when the space vector located in Sector 1, the desired volt-seconds are realized by applying the adjacent active vectors with switch configurations of [100], [110] for certain fractions of the sampling period T_s respectively and the zero vector (either [000] or [111]) for the remaining fraction of the sampling period. This strategy can be adapted to synthesize the desired output voltages from the high frequency sinusoidal link voltage obtained with the proposed inverter.

$$\overrightarrow{V_s} = v_{an}(t)e^{j0} + v_{bn}(t)e^{j\frac{2\pi}{3}} + v_{cn}(t)e^{j\frac{4\pi}{3}} \tag{2.6}$$

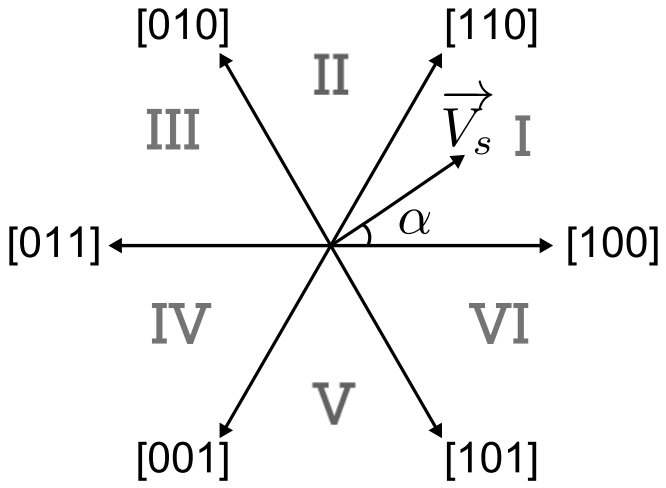

Figure 2.8: Space Vector Diagram

The switching of the H-bridge results in a high frequency sinusoidal voltage, v_{hf} across the secondary terminals of the transformer. This voltage has two zero crossings in one complete cycle. In order to achieve zero voltage switching, any change in the switch states of the secondary converter is restricted to the zero crossings of this link

voltage. Thus one complete half cycle of v_{hf} is the basic unit of voltage used to synthesize the output space vector. The volt seconds available in one half cycle of the link voltage are given by

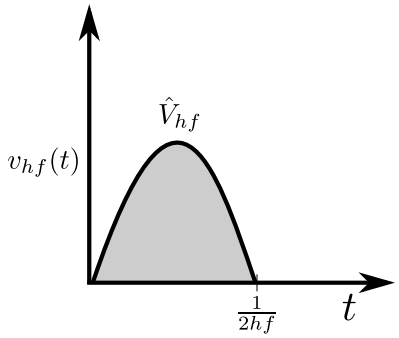

Figure 2.9: Volt Seconds

$$\int_0^{1/(2f_{hf})} \hat{V}_{hf} \sin(\omega_{hf} t)\, d(t) \;= \frac{\hat{V}_{hf}}{\pi f_{hf}} \tag{2.7}$$

Here, $\hat{V}_{hf}$ is the peak value of the link voltage across the secondary winding. Assuming a transformer turns ratio of n_t, $\hat{V}_{hf}$ equals $n_t V_{dc}$ when using the SLL technique for modulating the H-bridge and the maximum modulation index. The output space vector is assumed to have a magnitude $|\overrightarrow{V_s}|$ and rotates at a frequency f_0. Now for the given space vector $\overrightarrow{V_s}$, the desired volt seconds needed to make up the output voltage are realized by applying the adjacent vectors of Fig. 2.8 for some integral number of half cycles. In a sampling time interval of T_s, the expressions pertaining to the number of half cycles of vector [100], [110] and the zero vector [111] or [000] are given by dn_1, dn_2 and dn_0 respectively. The ratio of f_{hf} and the sampling frequency $f_s(= \frac{1}{T_s})$ is chosen to be an integer and is represented as m_f.

$$m_f = \frac{f_{hf}}{f_s} \tag{2.8}$$

$$|\overrightarrow{V_s}| \angle \alpha T_s = \frac{\hat{V}_{hf}}{\pi f_{hf}} \angle 0^0 dn_1 + \frac{\hat{V}_{hf}}{\pi f_{hf}} \angle 60^0 dn_2 \tag{2.9}$$

$$dn_1 + dn_2 + dn_0 = 2m_f \tag{2.10}$$

Solving the above equations, the following expressions are obtained

$$dn_1 = \pi \frac{f_{hf}}{f_s} \frac{|\overrightarrow{V_s}|}{\hat{V}_{hf}} \frac{\sin(60^0 - \alpha)}{\sin 60^0} \tag{2.11}$$

$$dn_2 = \pi \frac{f_{hf}}{f_s} \frac{|\overrightarrow{V_s}|}{\hat{V}_{hf}} \frac{\sin(\alpha)}{\sin 60^0} \tag{2.12}$$

The modulation index of the cycloconverter, m_v is defined as the ratio of the peak value of the output phase voltage to the peak value of the high frequency link voltage as shown in 2.13.

$$m_v = \frac{\hat{V}_{phn}}{\hat{V}_{hf}} \tag{2.13}$$

$$|\overrightarrow{V_s}| = \frac{3}{2} \hat{V}_{phn} \tag{2.14}$$

In a balanced three phase system, the absolute value of the space vector $|\overrightarrow{V_s}|$ is 1.5 times the peak value of the phase to neutral voltage 2.14. The values of $dn1$, $dn2$ and $dn0$ in a given sector can now be conveniently expressed as 2.17. The variation of the duty ratios with time is plotted in Fig. 2.10 and it shows that they are periodic over 60 degree intervals.

$$dn_1 = \sqrt{3}\pi m_f m_v \sin(60^0 - \alpha) \tag{2.15}$$

$$dn_2 = \sqrt{3}\pi m_f m_v \sin(\alpha) \tag{2.16}$$

$$dn_0 = 2m_f - dn_1 - dn_2 \tag{2.17}$$

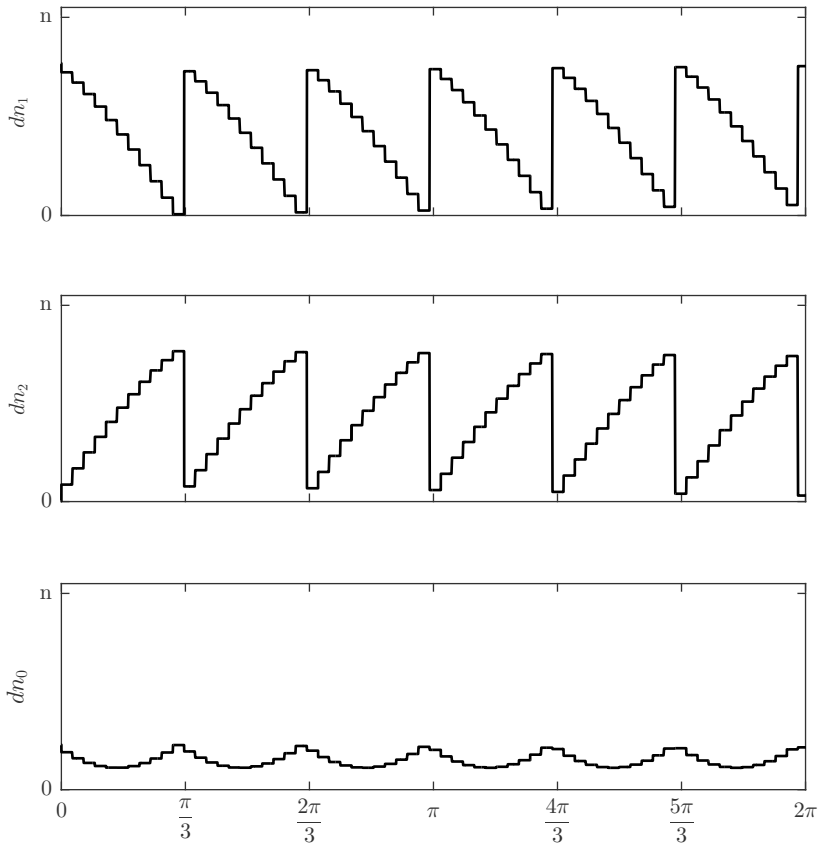

Figure 2.10: Duty ratio

The obtained values of dn_1, dn_2 and dn_0 are then compared against a sawtooth carrier comprising of discrete steps from 1 to $2\frac{f_{hf}}{f_s}$ as illustrated in Fig. 2.11. As long as the compared value is greater than the carrier signal, the appropriate switch is turned on. This is equivalent to rounding the obtained value to the previous integer and results in the application of integral half cycles of a switch combination. Given the high frequency nature of the link voltage, the error introduced by this type of rounding in time for applying a vector is quite low. A peak voltage detection circuit can be used to track any changes in the link voltage $\hat{V}_{hf}$ and appropriately adjust the half cycles required. A simple zero crossing detector circuit is used to track the polarity of the link voltage. When the link voltage is close to zero, the gate signals of the top switch and bottom switch in the legs of the cycloconverter are flipped. For instance, the state [100]

is realized for a negative value of link voltage by applying [011].

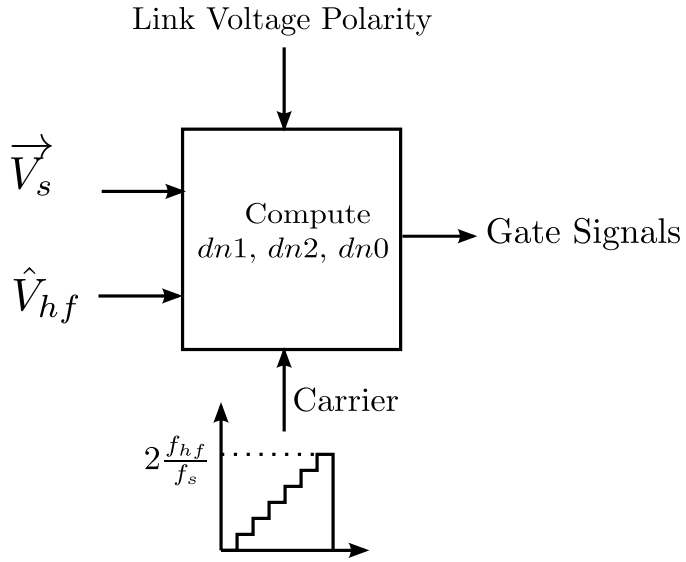

Figure 2.11: Generation of gate signals for cycloconverter

Fig. 2.12 shows the generation of the gate signal s_A for the phase leg A. The second plot in this figure shows the duty ratio of leg A in red being compared with the sawtooth carrier. When the duty ratio is greater than the carrier signal and the value of v_{hf} is positive, the value of s_A is equal to 1. Under similar conditions, if the voltage polarity of v_{hf} is negative, the value of s_A is set to 0. The plot of v_{AN} shows the voltage at the output of the phase leg A wrt the negative rail of the AC link denoted as N. The corresponding phase-neutral voltage of phase A is shown in v_{An}. The plots in Fig. 2.13 show the variation of the phase-neutral voltages of the three phases in a sampling interval of length T_s. The first plot shows the duty ratios of each phase leg and the staircase carrier. It can be seen that each T_s interval has regions where the voltage is either zero or has peak values of $+\text{-}\frac{2\hat{V}_{hf}}{3}$ or $+\text{-}\frac{\hat{V}_{hf}}{3}$. This variation occurs due to the effect of common mode voltage which is well understood.

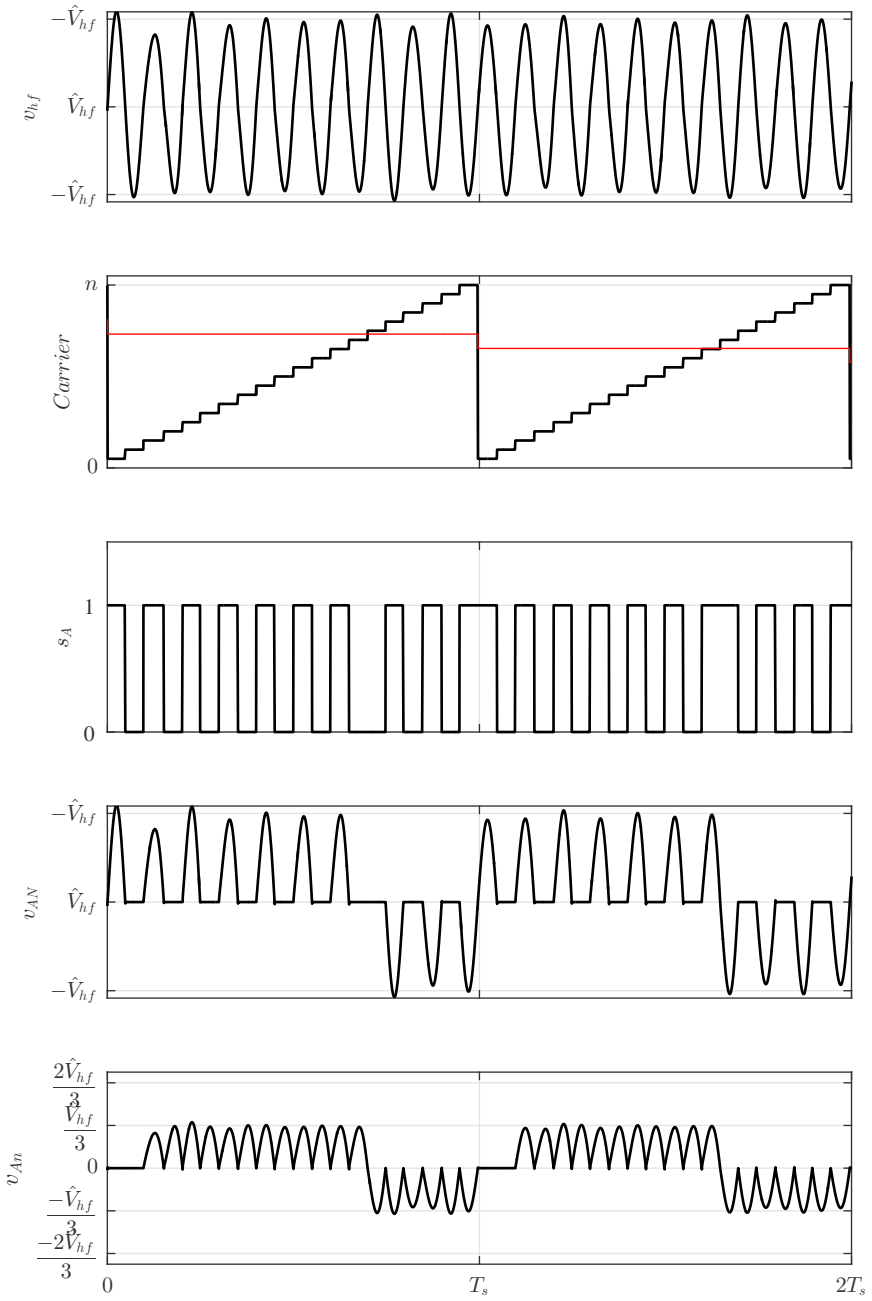

Figure 2.12: Duty ratio and switch signals

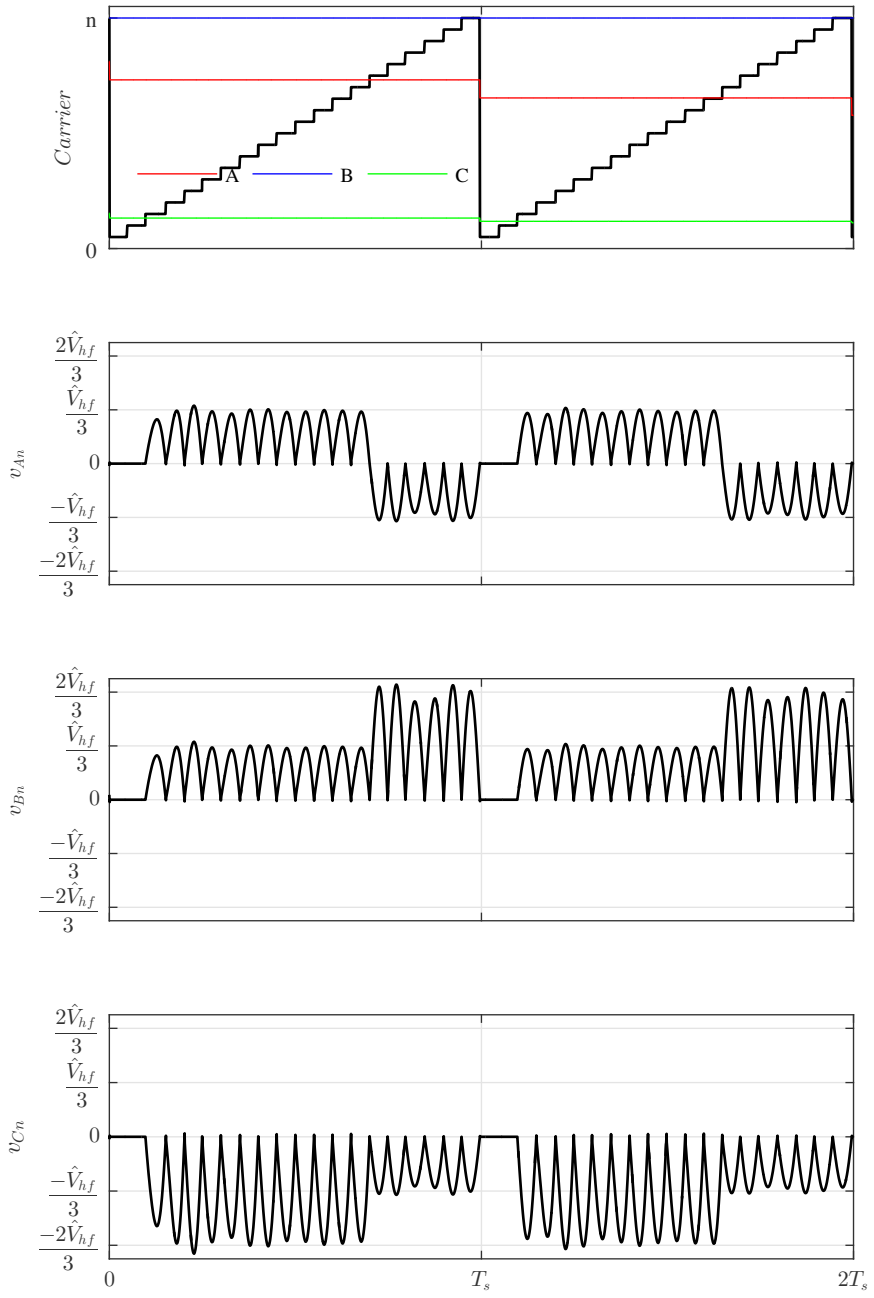

Figure 2.13: Duty ratios and phase-neutral voltages

2.4 Simulation Results

The proposed converter is simulated in the SIMULINK environment and the results showing the sinusoidal link current are presented. A transformer with a turns ratio of 1:2 is utilized and the DC input voltage is assumed to be 600V. The link frequency is fixed at 40kHz. The value of L_p is chosen as 28 μH and using (2.2), the value of C_p is calculated as 0.56 μF. An output voltage of 480V rms(LL), 60 Hz is synthesized to supply a load of 20kW at a load power factor of 0.8. The waveforms for one sampling period of the space vector are presented in Fig. 2.14. At a sampling frequency of 4kHz, one sampling interval spans 10 complete cycles of v_{hf} as shown. The current i_{switch} shows the input current drawn by the cycloconverter and has three distinct levels. The non-zero levels pertain to the instances where the two active vectors were being applied and the zero levels reflect the application of the zero vector. The value of this link current depends on the switching state of the cycloconverter. For the state [100], the magnitude of the current i_{switch} equals the phase a current of the load. This current is flipped in polarity every time the link voltage v_{hf} changes its polarity as can be seen from Fig. 2.14.

Table 2.1: Inverter Parameters

Parameter	Value
V_{dc}	600 V
$L_{lkg}(equvialent)$	20μH
Turns Ratio	1:2
f_{hf}	40kHz
f_s	4kHz
L_p	28 μH
C_p	0.56 μF
V_{phph}	480V rms
Output Power	20kW
Load Power Factor	0.8

The current i_{link} is the current passing through the secondary winding of transformer

and has the sinusoidal wave shape. As already stated, the parallel tank circuit acts as a low impedance path for the non-link frequency components of i_{switch} and only the link frequency component flows through the transformer. The current drawn from the dc voltage source, i_{dc} is also shown.

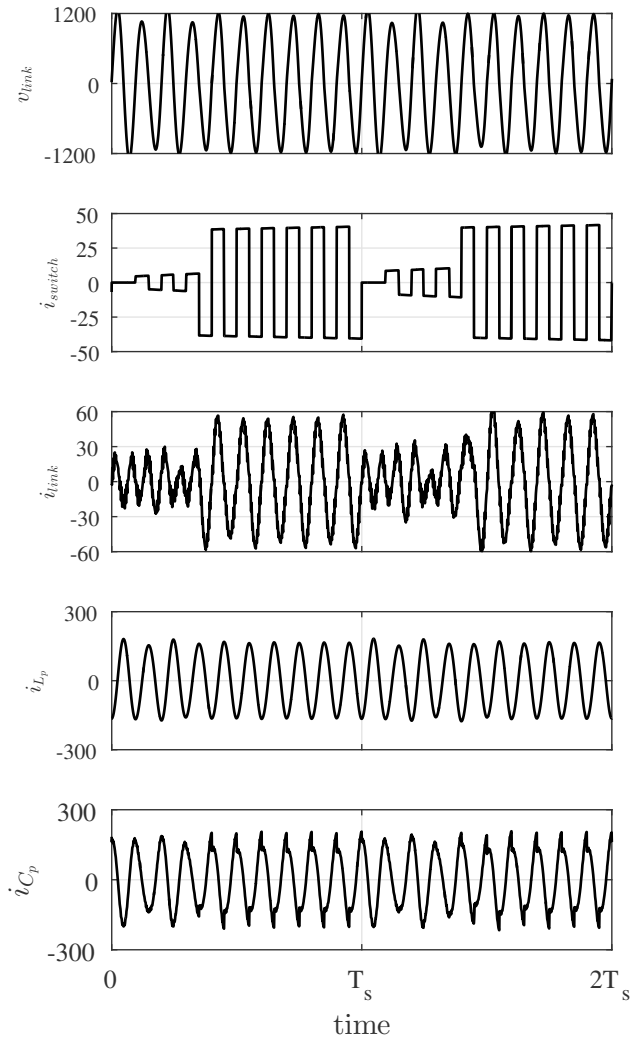

Figure 2.14: i) Voltage across the cycloconverter ii) Current at cycloconverter input iii) Current through transformer secondary winding iv) Current in inductor L_p v) Current in capacitor C_p

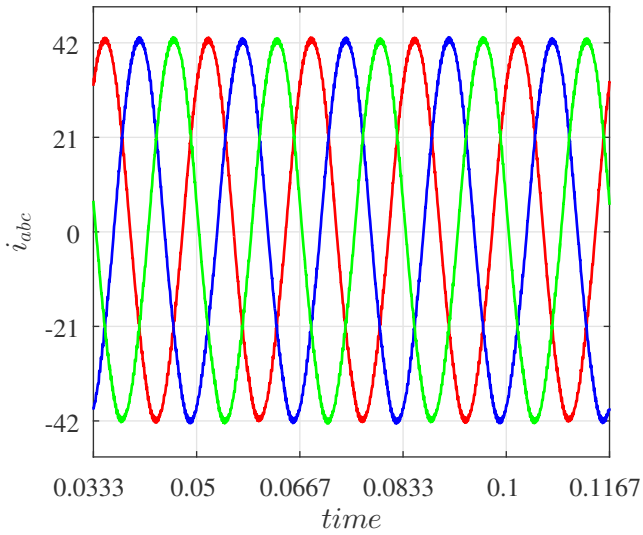

Figure 2.15: Output currents of the three phases

Fig. 2.15 shows the output phase currents and Fig. 2.16 shows the unfiltered phase to neutral voltage across the load. The phase-phase voltage waveshape is shown in Fig. 2.17. Fig. 2.18 shows a zoomed version of the phase to neutral load voltage comprised of sinusoidal half cycles. The variation in the link voltage, caused by the switched nature of the current from the cycloconverter, is reflected in the shape of the output phase voltage.

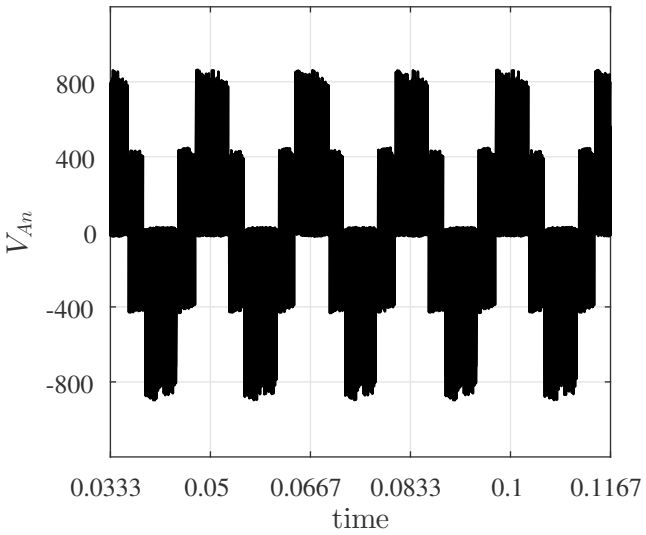

Figure 2.16: Phase to neutral voltage generated across the load

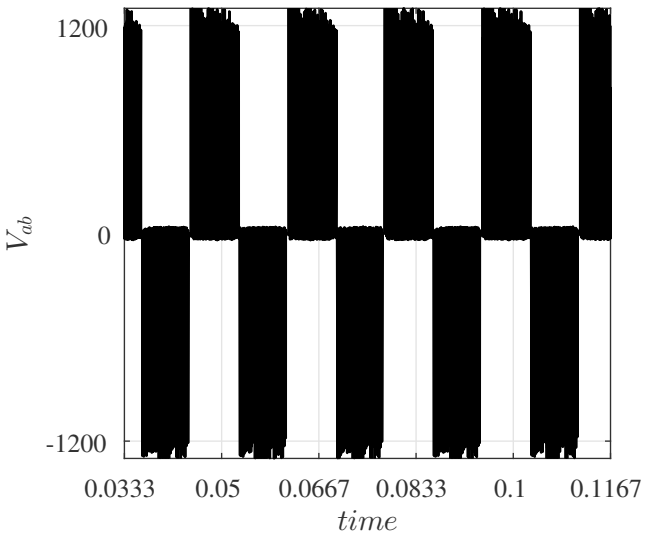

Figure 2.17: Line to line voltage

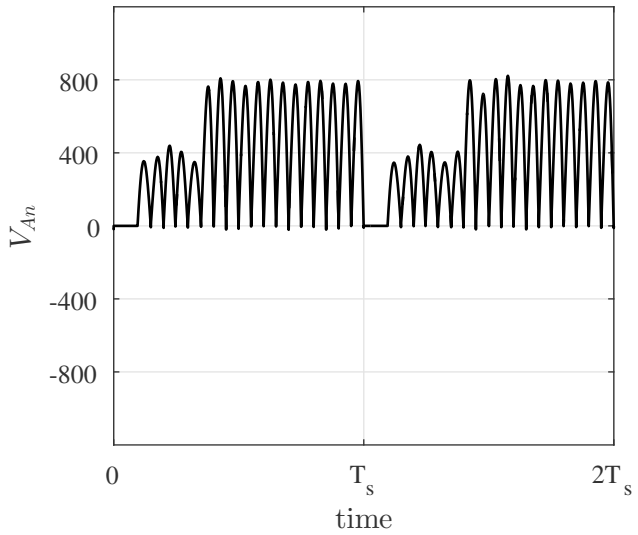

Figure 2.18: Zoomed phase to neutral voltage generated across the load showing the half cycles

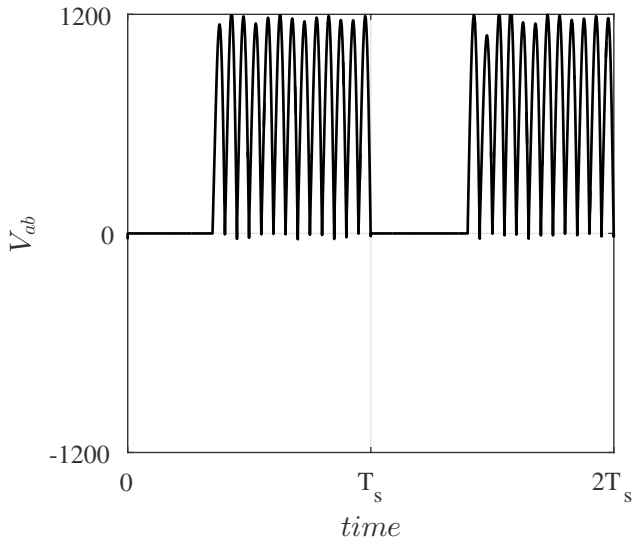

Figure 2.19: Zoomed phase to line-line voltage generated across the load showing the half cycles

The current through the primary winding of the high frequency transformer,i_{prim} is shown in Fig. 2.20. The current at the input of the H-bridge is a chopped version of

the primary winding current and has a sinusoidal envelope as shown in i_{DC}.

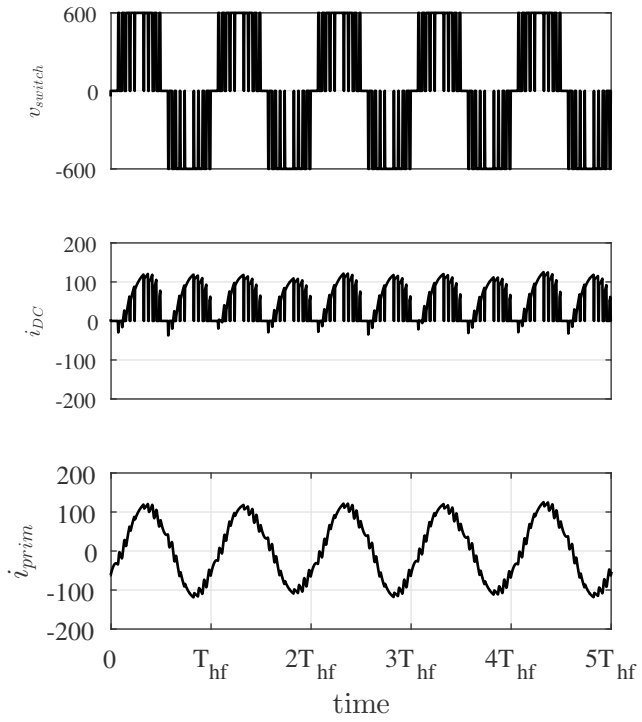

Figure 2.20: Plots showing the voltages and currents of the H-Bridge

A FFT of the the phase voltage is shown in Fig. 2.21 and shows the location of the switching harmonics. The first major group of harmonics occurs at the sampling frequency f_s and the next major group of harmonics is concentrated at twice the link frequency i.e $2f_{hf}$. Thus, a higher value of link frequency has the effect of shifting the second major group of harmonics even further away from the fundamental frequency. This is shown in Fig. 2.22 in which the sampling frequency is unchanged from Fig. 2.21 but the link frequency is now 80kHz instead of 40kHz. This is advantageous as it results in a smaller sized filter but increases the switching losses in the H-bridge.

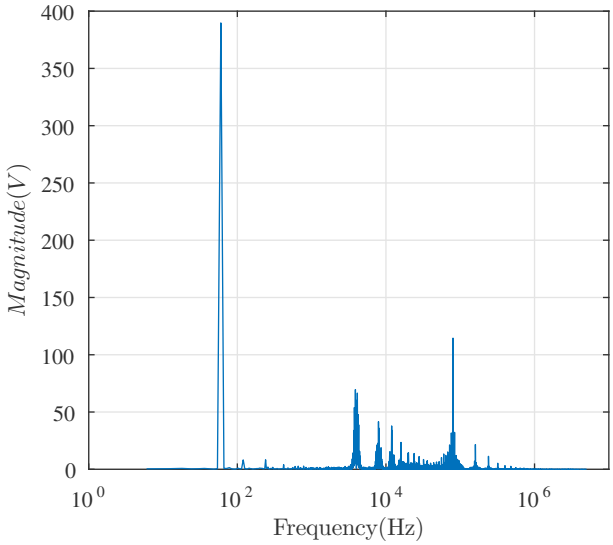

Figure 2.21: FFT of the voltage V_{An}

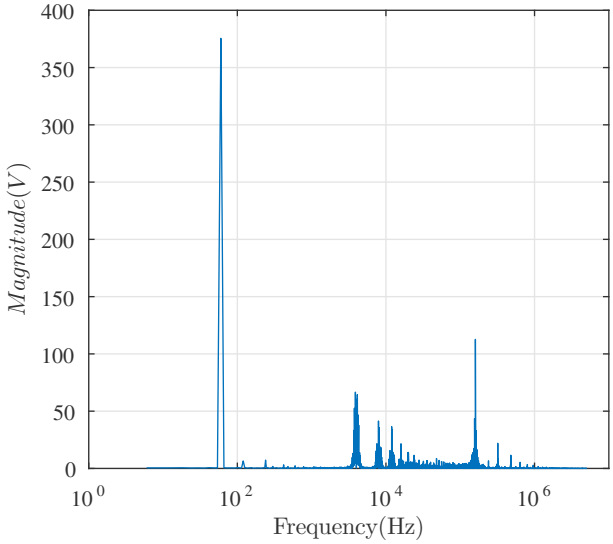

Figure 2.22: FFT of the voltage V_{An} when f_{hf} is 80kHz

2.5 Hardware Results

A hardware prototype was constructed to validate the proposed converter topology. The parallel LC tank is constructed using a $28\mu H$ inductance and a $4\mu F$ capacitor. The inductor used is manufactured by the company CWS and bears the part number ES55206-280M-160AH [56].This inductor uses a Sendust core and is well suited to carry large currents that are expected to flow within the tank. The capacitor is realized by paralleling the C4BSNBX4100ZAFJ series film capacitors which are manufactured by Kemet [57]. Each of these capacitors is rated at $1\mu F$ and four such capacitors are paralleled to obtain the desired capacitance of $4\mu F$.

A network analyzer was used to plot the impedance characteristics of the tank and the scan results can be seen in Fig. 2.24. The maximum impedance occurs at 15.92kHz and the phase at this frequency is almost zero. If the tank were constructed using an ideal inductor and ideal capacitor, the impedance would ideally be infinite at the resonant frequency. However, due to the finite Q factor of the tank, the maximum impedance occurs at 15.91kHz and differs from the expected value of 15.03kHz.

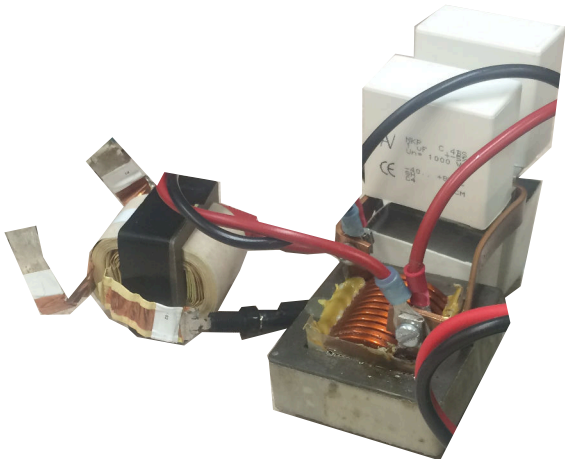

Figure 2.23: Highfrequency transformer and LC tank

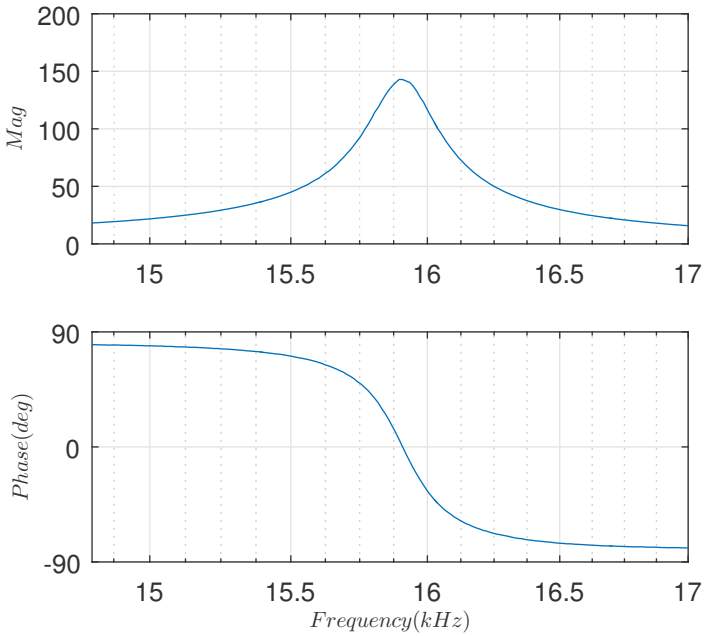

Figure 2.24: Impedance of LC Tank

When choosing the link frequency of the converter, it should be noted that f_{hf} should be that frequency at which the combination of transformer and LC tank exhibits the maximum impedance when seen from the primary terminals of the transformer. A network analyzer is used to measure the impedance at the primary winding of the transformer with the LC tank connected across the secondary. It can be seen that the maximum impedance occurs at 16.4kHz. This is due to the effect of the magnetizing inductance L_{m_p} which shifts the frequency at which the maximum impedance occurs. As a result, 16.4kHz is chosen as the frequency of the AC link to get minimum circulating current into the tank. The sampling frequency, f_s of the converter is chosen to be 4.1kHz such that the $\frac{f_{hf}}{f_s}$ ratio is an integer measuring 4. Thus one sampling interval over which the output voltage is synthesized has n=8 half cycles of the link voltage.

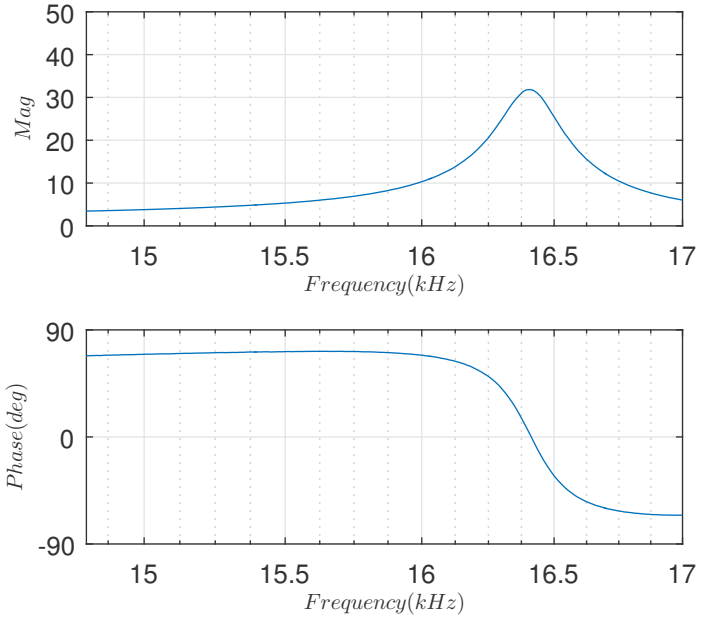

Figure 2.25: Impedance at primary winding

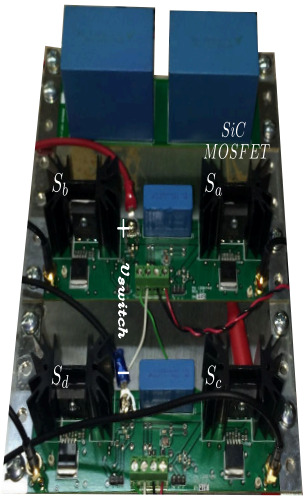

Figure 2.26: H Bridge

The H Bridge was built using SiC MOSFETs to synthesize the SHE PWM voltage with a fundamental frequency of f_{hf}. Two half bridges which use the SCH2080KE SiC MOSFET are used to form the H Bridge as show in Fig. 2.26. The high switching

frequencies supported by SiC devices make them the ideal candidate for this application. A dead time of 100nsec is incorporated to prevent accidental shoot through states when switching the legs.

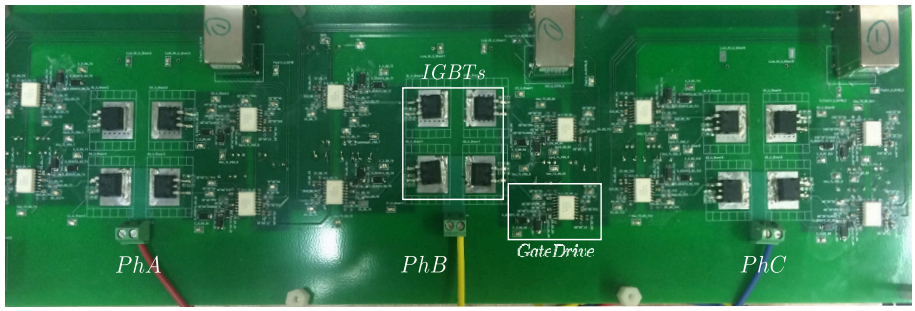

Figure 2.27: Hardware

Table 2.2: Hardware Prototype

Parameter	Value
$Switch\, S_a - S_d$	SCH2080KE
$Switch\, S_{AP} - S_{CN}$	STGB7NC60HDT4
V_{dc}	75 V
Turns Ratio	1:2
f_{hf}	16.4kHz
f_s	4.1kHz
$L_{lkg}(equvialent)$	20μH
L_p	28 μH
C_p	4 μF
Output Power	500W
Load Power Factor	0.8

The cycloconverter was constructed using discrete IGBT's which are connected in a common emitter configuration to realize a switch capable of blocking both positive and negative voltages. STGB7NC60HDT4 IGBT's from ST Microelectronics in a D2PAK package were used in the hardware prototype. These switches change their states only at the zero crossings of the link voltage and hence switching losses are almost negligible.

The IGBT's are driven using ACPL 332J drivers from Avago with a gate resistance of 20 Ω. These drivers offer optical isolation and fault protection. Each phase of the cycloconverter is comprised of four discrete IGBT's and their associated circuitry as seen in Fig. 2.27. The operation of the hardware prototype can be verified from the results presented in Fig. 2.28 and 2.29.

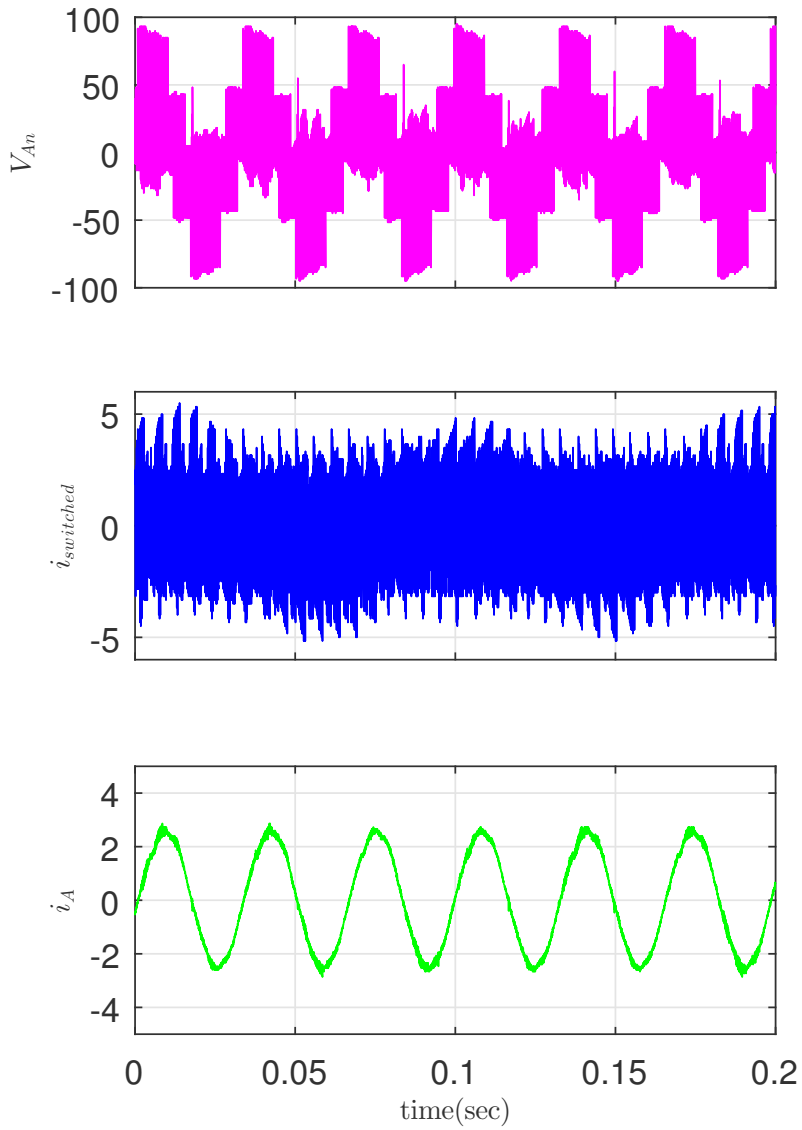

Figure 2.28: Phase voltage, switched current and the load current of the hardware prototype

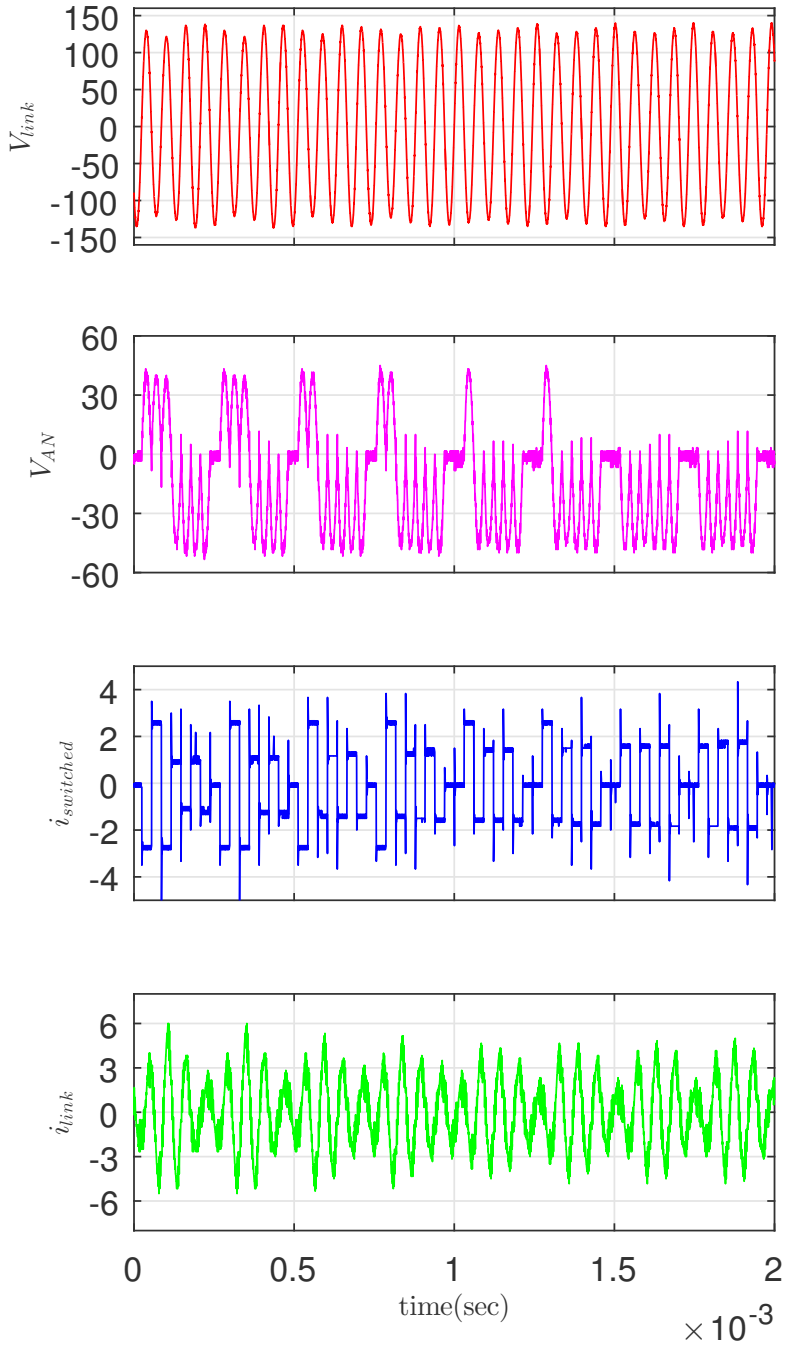

Figure 2.29: Link waveforms of the hardware prototype

The Fourier spectrum of the phase to neutral voltage is presented in Fig. 2.30a. It

can be seen that the harmonics occur at multiples of the sampling frequency f_s and at twice the link frequency i.e $2f_{hf}$. It can be inferred that using a higher value of the link frequencies would push these harmonics much farther away from the fundamental frequency. The Fourier spectrum of the currents i_{switch} and i_{link} are shown in Fig. 2.31a and 2.31b respectively.

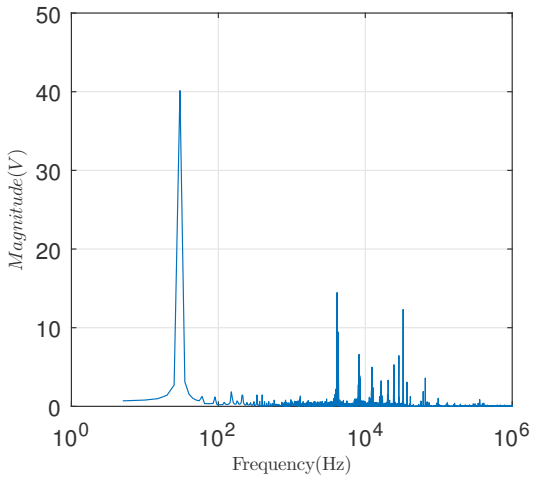

(a)

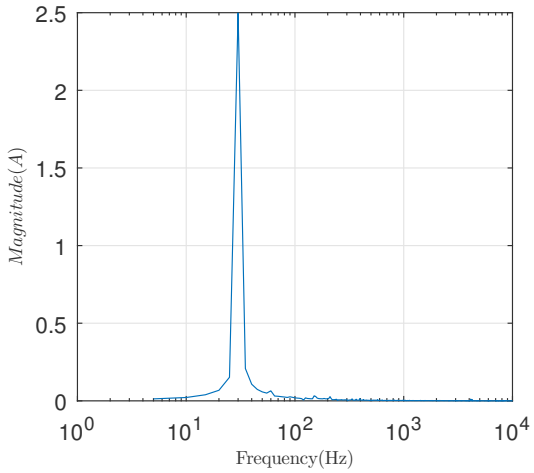

(b)

Figure 2.30: (a) FFT of v_{An} (b) FFT of the load current

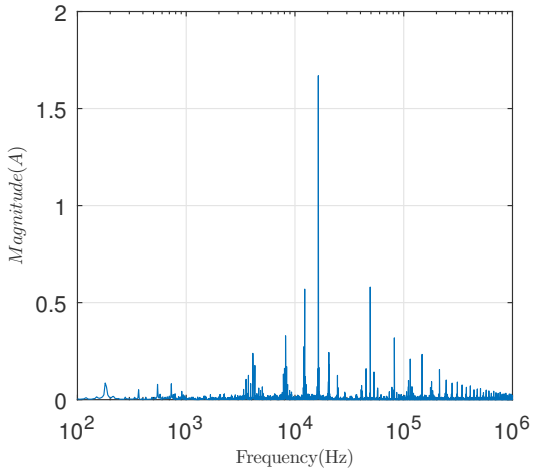

(a)

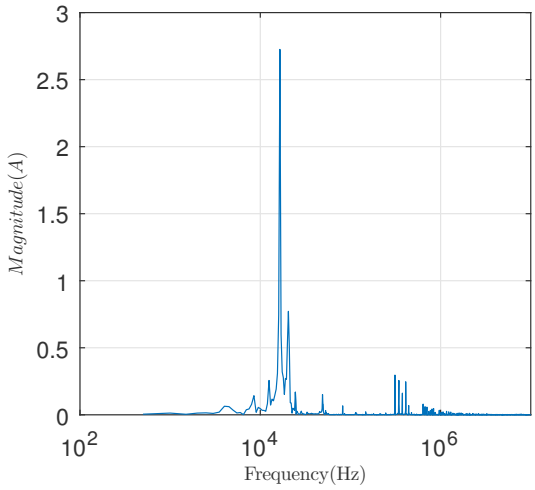

(b)

Figure 2.31: (a) FFT of switched current (b) FFT of link current

2.6 Commutation

The cycloconverters are constructed using IGBT's connected in the common emitter configuration to obtain switches capable of blocking voltage of either polarity. Consequently, when switching between the top and bottom bidirectional switch in a leg, four

step commutation technique needs to be used to ensure that there is always a safe path for the phase currents to flow [35]. Based on the polarity of the phase current, the entire process of transferring the current from the top switch to the bottom switch is accomplished in four discrete steps. This is illustrated in Fig 2.32 where the states of the four individual devices S_{1x}, S_{2x}, S_{3x} and S_{4x} that constitute one bidirectional leg are shown during the transition from ON state to OFF and vice versa. The states to the left of the dotted line refer to the case when $i > 0$ i.e current is flowing out of the leg while states to the right of the dotted line occur when the current is flowing into the leg.

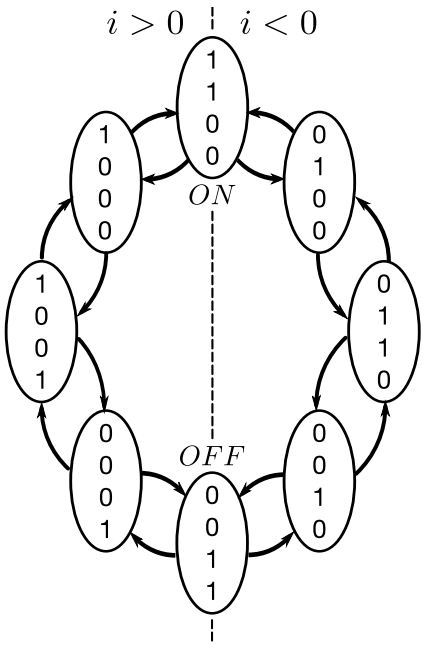

Figure 2.32: Four step commutation

2.7 Summary

This chapter demonstrated a high frequency ac link three phase inverter that avoids the problem of the leakage energy commutation by using a parallel LC tank. The use of a resonant tank circuit with small values of reactive elements ensures that the size of the inverter can be compact. The modulation of the cycloconverter to generate the desired

outputs using a discrete space vector algorithm was explained. Zero voltage switching of the cycloconverter is another added benefit of the proposed scheme. This inverter can have higher link frequencies to take advantage of fast switching power electronic devices without being constrained by additional time otherwise needed for the commutation of leakage energy.

Chapter 3

High Frequency AC Link Transformer Isolated Open End Drive

3.1 Introduction

The majority of the variable speed drives used in industry utilize voltage source inverters (VSI) which have been thoroughly investigated over the years [58]. While the space vector modulation method is widely used, it causes unwanted bearing currents which lead to the eventual failure of the drive. Open end winding configuration of electric motors utilizing dual VSIs has been proposed as a way to avoid bearing currents [59,60].

However, a major drawback of the DC link based VSI configuration is that the electrolytic capacitors used to construct the DC link tend to degrade with time. To avoid the need for such capacitors and improve the reliability of the drive, open end drive configurations based on matrix converters have been investigated in [61–64] where the matrix converters are modulated using synchronous rotating vectors to generate the desired outputs. Alternately, inverters utilizing a high frequency AC link offer an attractive solution for use in open end drives by eliminating the need for bulky electrolytic capacitors along with the added advantages of allowing the use of compact and light weight transformers to achieve galvanic isolation and voltage transformation.

This chapter extends the high frequency link scheme presented in the earlier chapter to realize an open end drive that uses dual cycloconverters to generate the necessary motor voltages[1] . It combines the advantages of an open end winding configuration and a high frequency ac link. The open end configuration leads to an improved utilization of the ac link and have the problem of leakage energy commutation which eliminates the need for lossy voltage clamping circuits. By restricting any change in the switch states of the cycloconverter to the zero crossing regions of the link, switching losses are avoided in the cycloconverter.

3.2 Bearing currents

The source of bearing currents in induction motors driven by PWM converters was explained by [66]. It was shown that multiple parasitic capacitances exist due to the construction of the induction machine. Due to the high rate of change in the switching voltages applied by PWM converters, these capacitances provide a path for common mode currents to flow through the system. Common mode currents can lead to EMC issues and may also corrupt low level signals. Moreover, the voltage buildup across the capacitances is discharged through the bearings which support the shaft leading to bearing currents. These cause the machines to fail over time as they result in mechanical wear and tear of the bearings [4]. It can be seen that the high $\frac{dv}{dt}$ of the switching voltages applied by PWM converters can lead to several problems in the system.

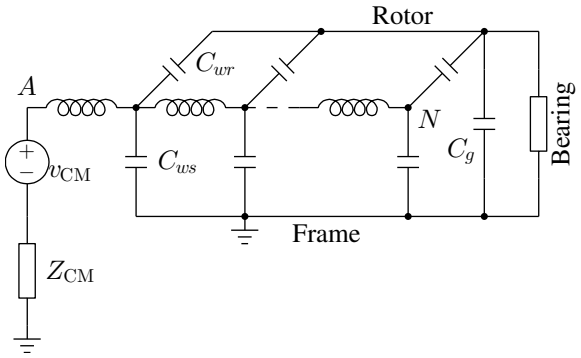

Figure 3.1: Common mode circuit of a drive

[1] Parts of this chapter are taken from [65]

The common mode voltage in a system defined as follows

$$V_{CM} = \frac{V_{AN} + V_{BN} + V_{CN}}{3} \tag{3.1}$$

Suppression of shaft voltages and bearing currents can be done either by modifying the modulation scheme used or by altering the impedance of the common mode current paths as explained in [67]. The use of multilevel inverter PWM schemes was presented in [67] to eliminate common mode voltages. The paper proposed that only certain switching states be selected by the modulation algorithm such that the generated common mode voltage is zero. Alternately, [68] proposed the addition of active circuit that applies voltages whose common mode voltage has the opposite polarity. As reported by [69], dual VSI fed open end drives can also be used to eliminate the common mode voltages. This scheme ensures that the switching states of the dual VSI's result in the same common mode voltage across the machine stator windings. The use of open end drives also leads to an improved modulation index i.e a smaller bus voltage is needed to generate a given output voltage.

3.3 Description of the Converter

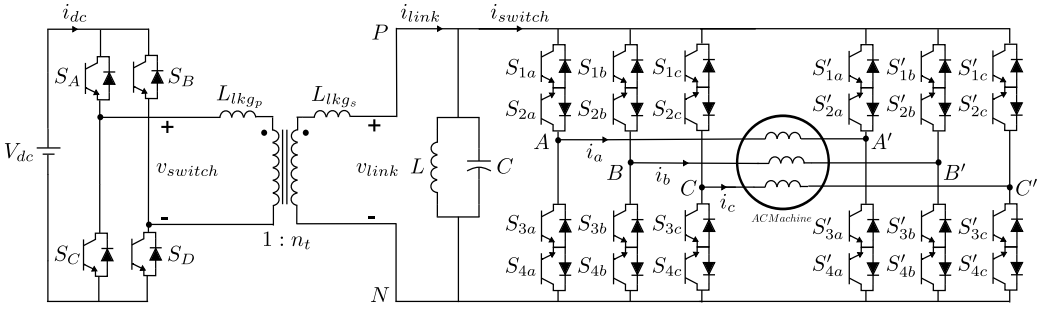

Figure 3.2: High frequency transformer Isolated AC link open end drive

The proposed high frequency ac link open end drive is shown in Fig 3.2. An H-bridge comprising of switches S_A through S_D is used to generate a high frequency AC waveform at a frequency f_{hf} from a DC voltage source. A high frequency transformer with a turns ratio of n_t is connected in the link and L_{lkg_p} and L_{lkg_s} are the leakage inductances of

the transformer windings. A parallel tank comprising of inductor L and capacitor C is connected across the secondary winding of the transformer. The resonant frequency of the tank, given by $f_r = \frac{1}{2\pi\sqrt{LC}}$ is designed to be equal to f_{hf}. The terminals of the open end machine are fed from two cycloconverters comprising of switches S_{1a} through S_{4c} and S'_{1a} through S'_{4c} respectively. These switches need to be capable of blocking the alternating link voltage and hence should have bidirectional voltage blocking capability. This can achieved by connecting two IGBT's in a common emitter scheme as shown. An open end winding configuration in an induction machine is obtained by opening the neutral point of the stator windings in a regular induction machine. In the following sections, it is assumed that the switches are ideal and the magnetizing inductance of the transformer is very large and can be neglected.

3.4 Principle of Operation

The switching of the H bridge and the use of a parallel tank circuit have been previously explained. A SHE modulation technique is employed for the generation of a high frequency AC link. The modulation index of the H bridge is selected to generate AC link voltage of maximum amplitude i.e $m_{vH} = 1$. The operation of the dual cycloconverters to generate variable frequency motor voltages is now explained.

3.4.1 Open End Drive Operation

An open-end winding induction motor is realized by opening the neutral point of the stator windings of a regular induction motor. This provides access to three additional motor terminals which are fed from a separate three phase converter. When utilizing a DC-link based open end drive, the two pairs of motor terminals are fed by voltage source inverters(VSI). The space vector modulation technique for an open drive using dual VSI's has been described in [70]. A major advantage of the open end configuration is that it requires the use of only half the bus voltage as a single end configuration to generate a given output voltage. The possible voltage vectors of the VSI's can be represented using the space vector diagram as shown in Fig. 3.3a and 3.3b. The switch states to obtain the voltage vector are also shown. The common mode voltage of a switch combination, V_{CM}, is defined as (3.1).

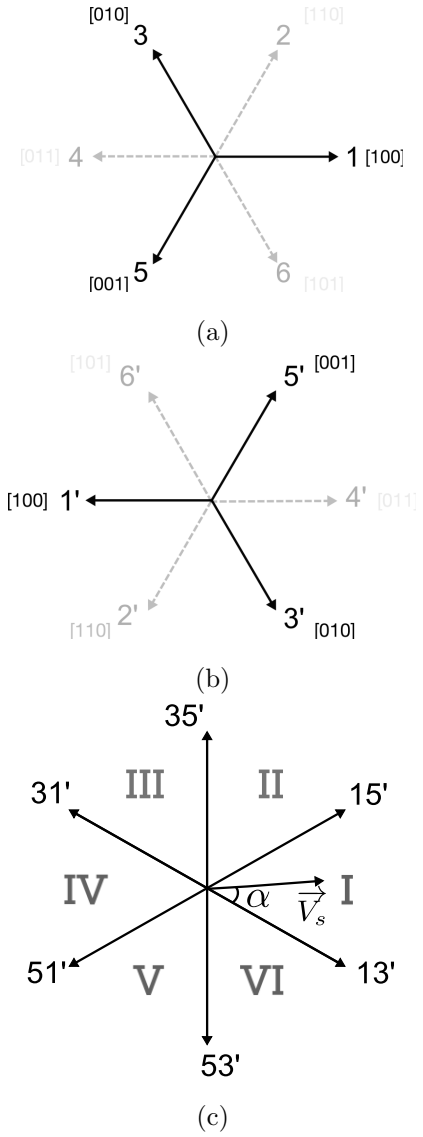

Figure 3.3: (a) & (b) Space vector diagrams of the cycloconverters showing the vectors with similar common mode voltage (c) Resultant voltage vectors of the open end configuration

The active vectors in a VSI have either one phase connected to the positive DC bus or two phases connected to the positive DC bus. Hence, the common mode voltage generated by the active vectors of a VSI with a DC bus value of V_{DC} is either $\frac{2V_{DC}}{3}$ or

$\frac{V_{DC}}{3}$. If two active vectors with different common mode voltage are applied on either end of the open end drive, it zero sequence currents to flow through the machine windings. This is undesirable and leads to a reduction in efficiency. It is known [70] that the use of isolated voltage sources for each of the VSIs can help these zero sequence currents. Rather than using isolated voltage sources, the modulation strategy can be restricted to utilizing active vectors with the same common mode voltage to avoid zero sequence currents [69].

3.4.2 Modulation of the Cycloconverters

A constant common mode voltage across the phase windings can be achieved by utilizing vectors which have the same common mode voltage as described in [60]. It can be seen that vectors **1,3,5** possessing the switch states $S_aS_bS_c$ as [100], [010] and [001] respectively have the same V_{CM}. The switch state '[100]' means the top bidirectional switch in Phase A is ON and the bottom bidirectional switches in Phase B and C are ON. The zero vector is constructed using one of the combinations of **11',33',55'** to ensure that V_{CM} remains constant. It should be noted that using the vectors **2,4,6** will also yield similar results. The resulting voltage vectors possible by using the **1,3,5** vectors and **1',3',5'** vectors that generate the same common mode voltage on either end of the motor windings are shown in Fig. 3.3c along with the desired output voltage space vector,$\overrightarrow{V_s}(t)$. The vector 13' means that cycloconverter 1 has a switch state of [100] while cycloconverter 2 has a switch state of [010].

Depending on the sector in which $\overrightarrow{V_s}(t)$ lies, the voltage is synthesized by applying two adjacent active vectors and a zero vector for specific time periods within a given sampling period. For the ac link case, this is implemented by considering the volt-seconds available in one sinusoidal half-cycle of the link as the fundamental unit to synthesize the output during a sampling period T_s. The volt-seconds in one half cycle of the link voltage are given as $\varphi = \dfrac{\hat{v_{hf}}}{\pi f_{hf}}$. For a given vector V_{mn} where $m \epsilon 1,3,5$ and $n \epsilon 1',3',5'$, let S_{mx} and S_{nx} be switch states of the cycloconverter legs respectively where $x \epsilon a,b,c$. The volt-seconds of the vector V_{mn} are calculated as shown in (3.2).

$$\overrightarrow{V_{mn}} = \varphi((S_{ma} - S_{na})e^{j0} + (S_{mb} - S_{nb})e^{j\frac{2\pi}{3}} + (S_{mc} - S_{nc})e^{j\frac{4\pi}{3}}) \tag{3.2}$$

$$|\overrightarrow{V_s}|\angle\alpha T_s = V_1 dn_1 + V_2 dn_2 + V_0 dn_0 \tag{3.3}$$

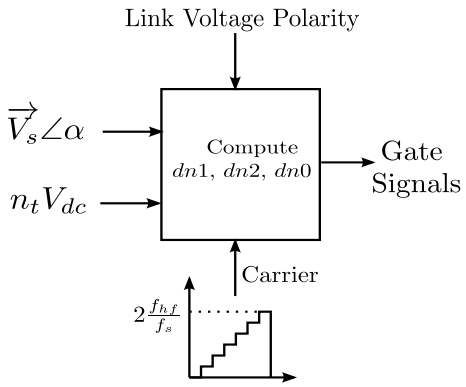

Figure 3.4: Generation of gate signals

The output voltage is synthesized during the time T_s by applying an integral number of half-cycles of two adjacent active vectors, say dn_1 and dn_2, and using a zero vector for the remaining time given by dn_0 as given by (3.4). By applying an integral number of half cycles, it is ensured that the output switches always change state when the voltage across them is very low and resulting in negligible switching loss. From (3.4), the resulting length of the vectors in Fig. 3.3c is calculated as $\frac{\sqrt{3}n_t V_{dc}}{\pi f_{hf}}$ and it can be shown that the maximum value of m_v, where $m_v = \frac{\hat{V}_o}{n_t V_{dc}}$, of this configuration is 0.6366 which is higher than the maximum value of m_v of a similar single end configuration which is 0.3675. Thus, using an open end configuration allows the generation of larger output voltages from a given ac link and reduces the component stresses.

$$\begin{gathered} dn_1 = \pi m_v m_f \sin(60^0 - \alpha); \\ dn_2 = \pi m_v m_f \sin(\alpha); \\ dn_0 = 2 * m_f - dn_1 - dn_2; \\ \text{where} \quad f_s = \frac{1}{T_s}; \quad \hat{V_o} = \frac{2}{3}|\overrightarrow{V_s}|; \quad \text{and} \quad m_f = \frac{f_{hf}}{f_s} \end{gathered} \tag{3.4}$$

The obtained values of dn_1, dn_2 and dn_0 are then compared with a sawtooth carrier with discrete levels ranging from 0 to $2m_f$ as shown in Fig. 3.4 to get the appropriate

gate signals. The switch states of the cycloconverters are reversed every time the link voltage polarity changes.

The current i_{switch} depends on the vector combination applied and the values of the three phase currents at that instant. Assuming the load current to be inductive and at a much lower frequency than f_{hf}, the effect of reversing the switch states is the polarity reversal of i_{switch} resulting in the switched waveshape.

3.5 Results

The converter described above was simulated in the $SIMULINK$ environment by considering a transformer with leakage inductance of 20 μH and a link frequency of 15kHz and supplying 20kW of power at a load power factor of 0.8. The value of V_{dc} was assumed to be 600V and n_t=1. The modulation index was set to 0.56 to generate a line voltage of 415V(RMS). The parallel tank is constructed using an inductor of 28 μH and a capacitance of $4\mu F$. The plot of i_{switch} in Fig. 3.5 shows different current levels corresponding to the application of different active vectors and the corresponding i_{link}. The output currents and the voltage $V_{AA'}$ are shown in Fig. 3.7a and 3.6. It can be observed that the phase voltage is composed of sinusoidal half cycles of the ac link.

A hardware prototype was constructed using STGB7NC60HDT4 IGBTs configured in a common emitter configuration for switches S_{1a} through S'_{4c} and SCH2080KE power MOSFETs for switches S_A-S_D. The DC bus was set at 50V to achieve a no-load peak link voltage of 100V. A modulation index of 0.56 was assumed and a 30Hz output was generated across a static RL load with R=10 Ω and L=45.8 mH. Current sensors are used to sense the polarity of load currents to implement four step commutation which is necessary to switch the bidirectional switches. The results are shown in Fig. 3.10

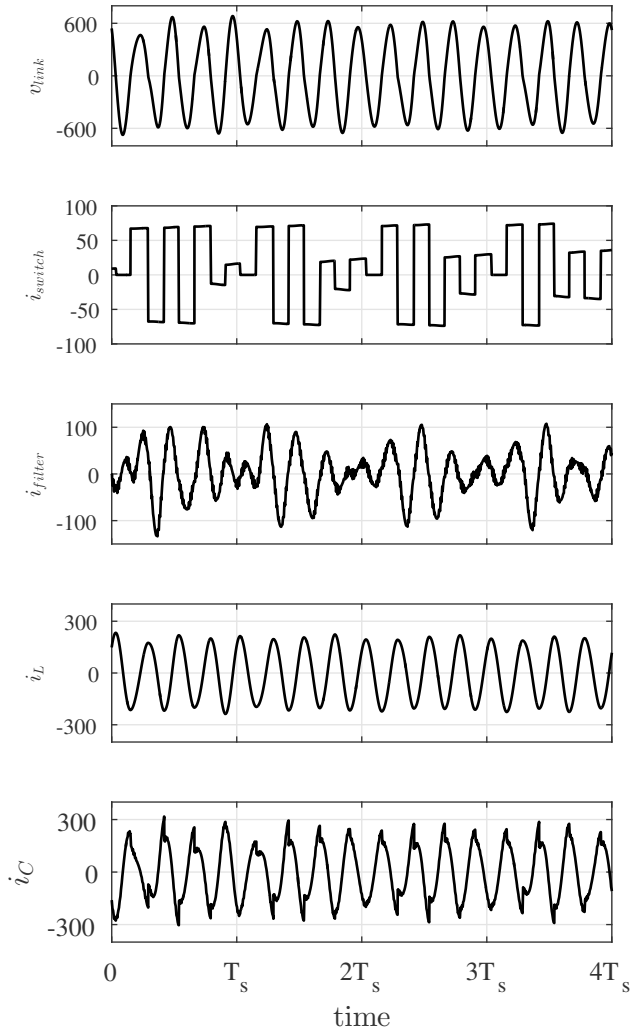

Figure 3.5: Link waveforms of the open end drive

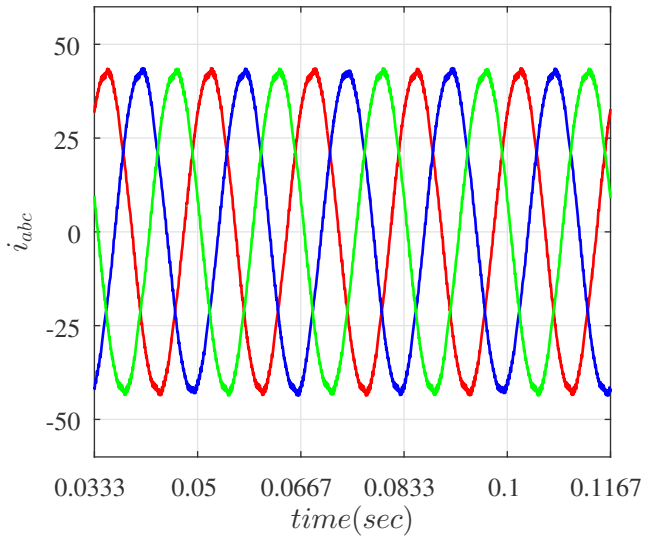

Figure 3.6: Three phase currents

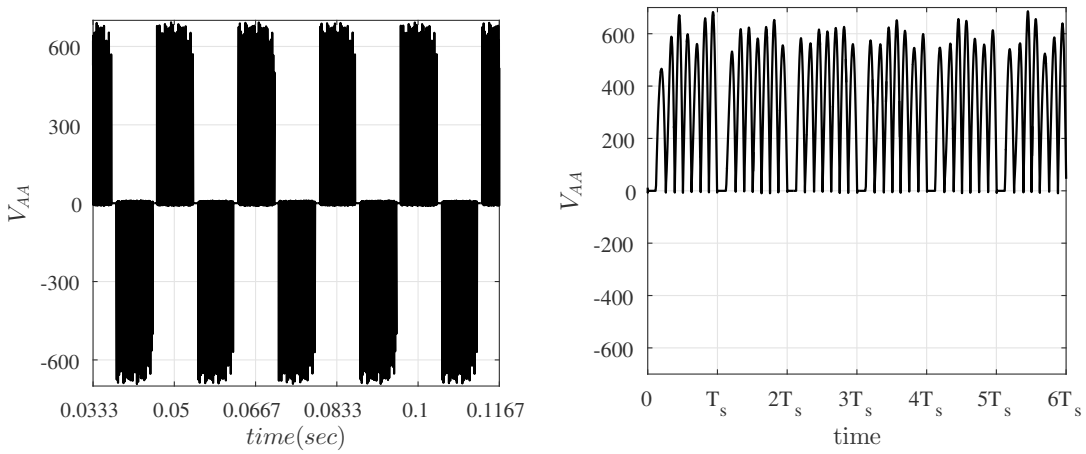

(a) (b)

Figure 3.7: (a) Phase voltage (b) Zoomed phase voltage

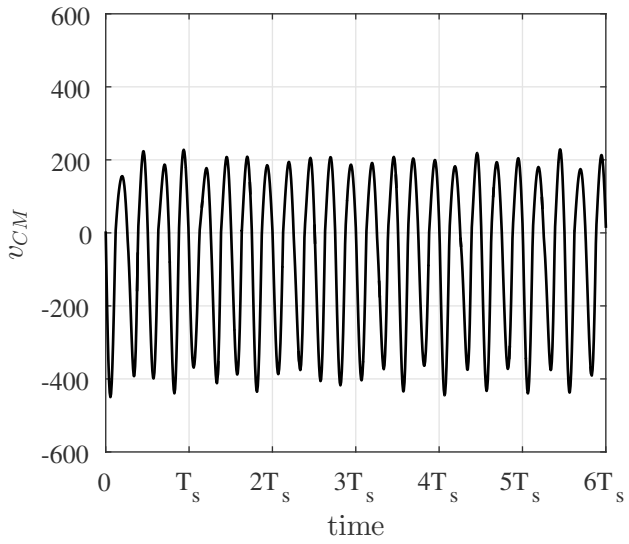

Figure 3.8: Common mode voltage

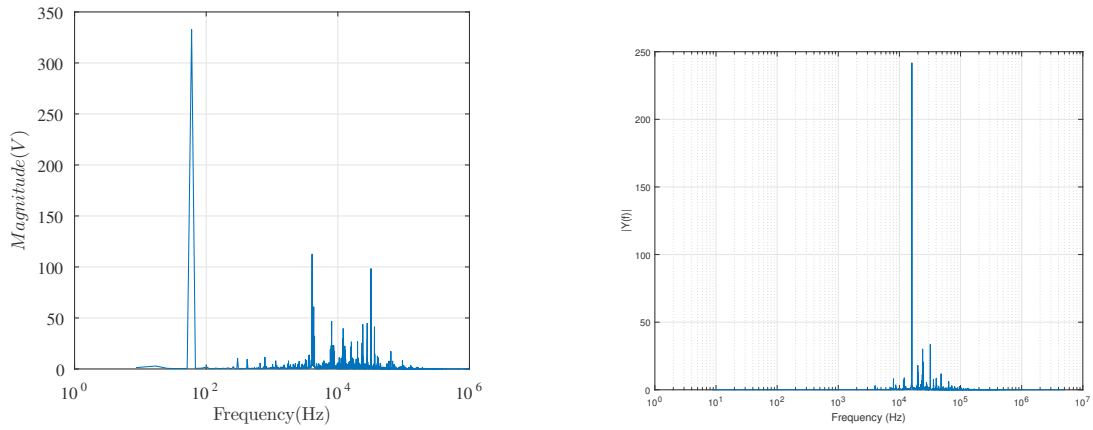

(a) (b)

Figure 3.9: (a) Fourier spectrum of the voltage v_{AA} (b) Fourier spectrum of the common mode voltage

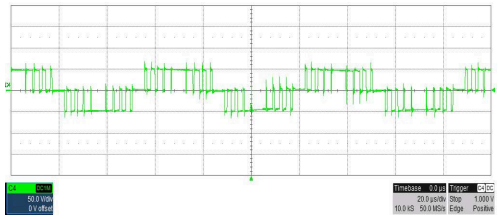

(a)

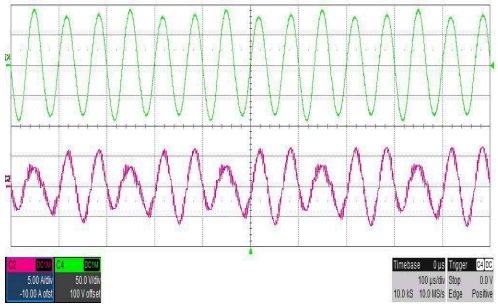

(b)

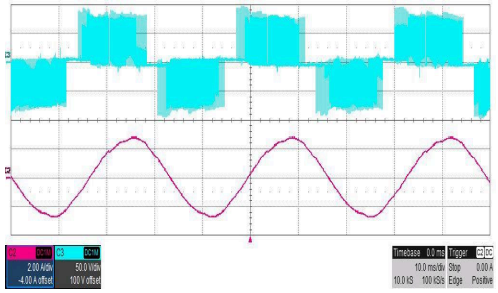

(c)

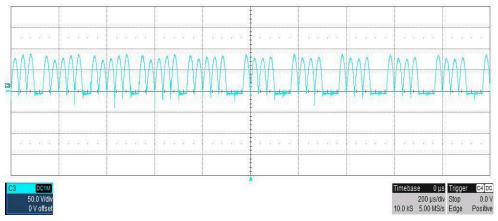

(d)

Figure 3.10: (a) Voltage across the primary winding (b) AC Link voltage and current (c) Output phase a current and voltage (d) Phase a voltage on an expanded time scale

Table 3.1: Electrical Parameters

Parameter	Value
Power	20kW
V_{dc}	600V
V_{out}	415V(RMS)
L	28μH
C	3.53μF
L_{Lkg}	20μH
n_t	2

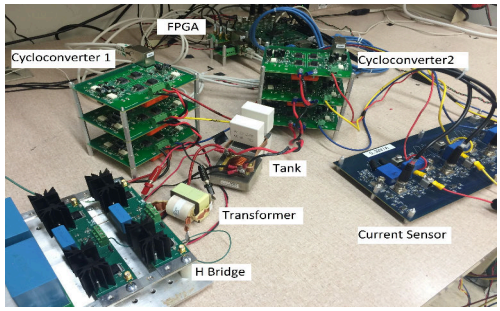

Figure 3.11: Hardware prototype

3.6 Variable gain of H Bridge

In the preceding sections, it was assumed that H bridge is modulated so that it generates a SHE voltage and the peak value of the fundamental voltage is the same as V_{DC}.The modulation index of the H bridge m_{v_H} as defined in 3.5 is maintained at unity and the magnitude of v_{link} under all operating conditions is constant. The output voltage was changed by controlling the modulation index m_v of the cycloconverter. Alternately, m_{v_H} of the H bridge can be controlled to adjust the magnitude of output voltage as illustrated in Fig. 3.12.

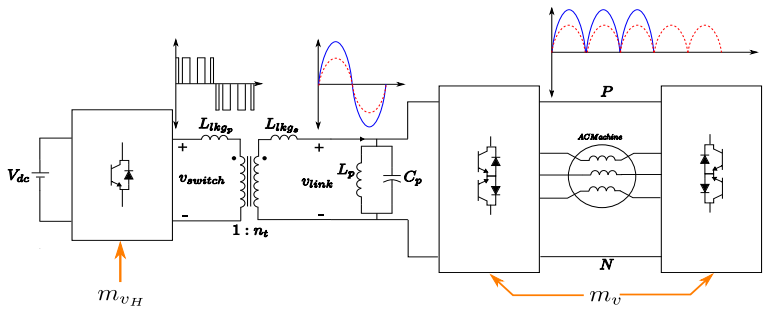

Figure 3.12: Output voltage control through m_{v_H}

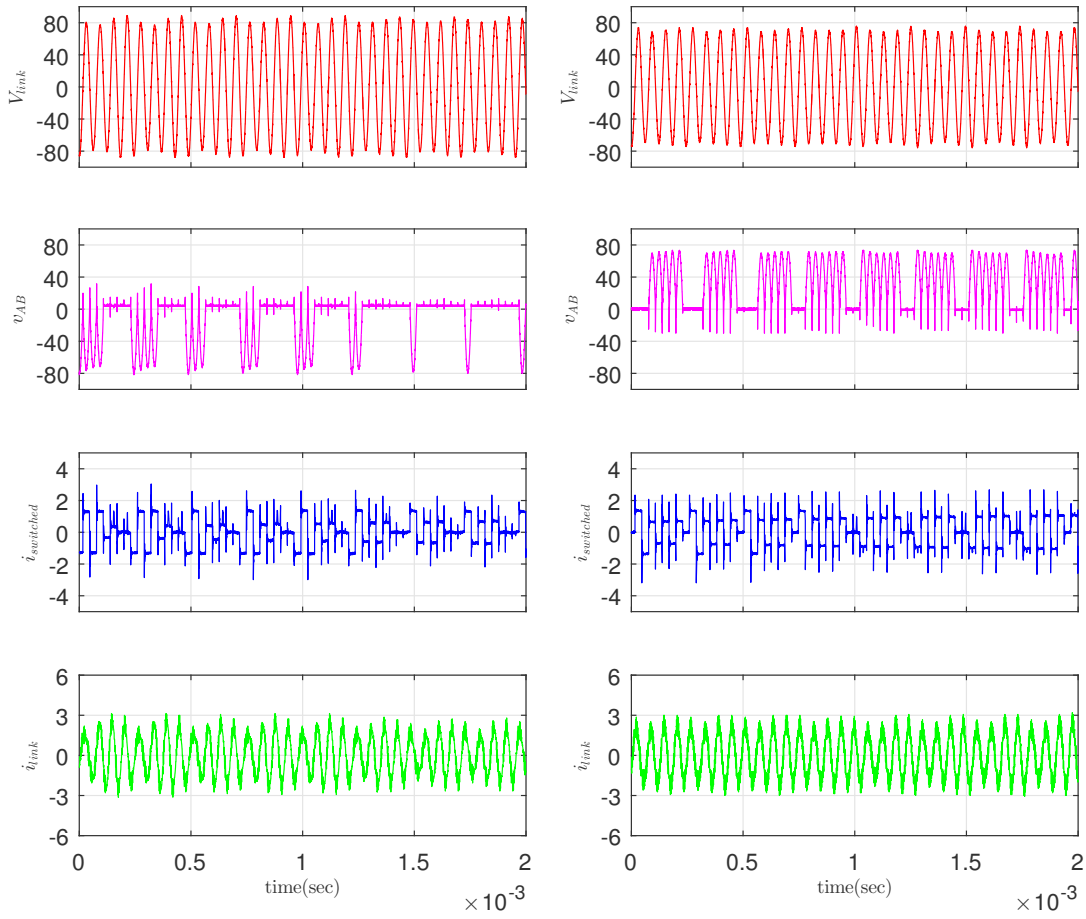

Figure 3.13: (a) Link waveforms with m_{v_H}=1 (b) Link waveforms with reduced m_{v_H}

$$m_{v_H} = \frac{\hat{V}_{hf}}{V_{DC}} \tag{3.5}$$

In this alternate control scheme, the cycloconverter is operated with the maximum value of modulation index and instead, the value of m_{v_H} is varied. The ac link voltage magnitude is changed by using the appropriate switching angles to still achieve selective elimination of harmonics in v_{switch}. The switching angles for a range of values of m_{v_H} can be pre-calculated and stored in a lookup table. This approach has the following benefits :

- reduced iron losses in the transformer and the machine due to reduced voltage magnitude
- reduced magnitude of currents circulating within the tank

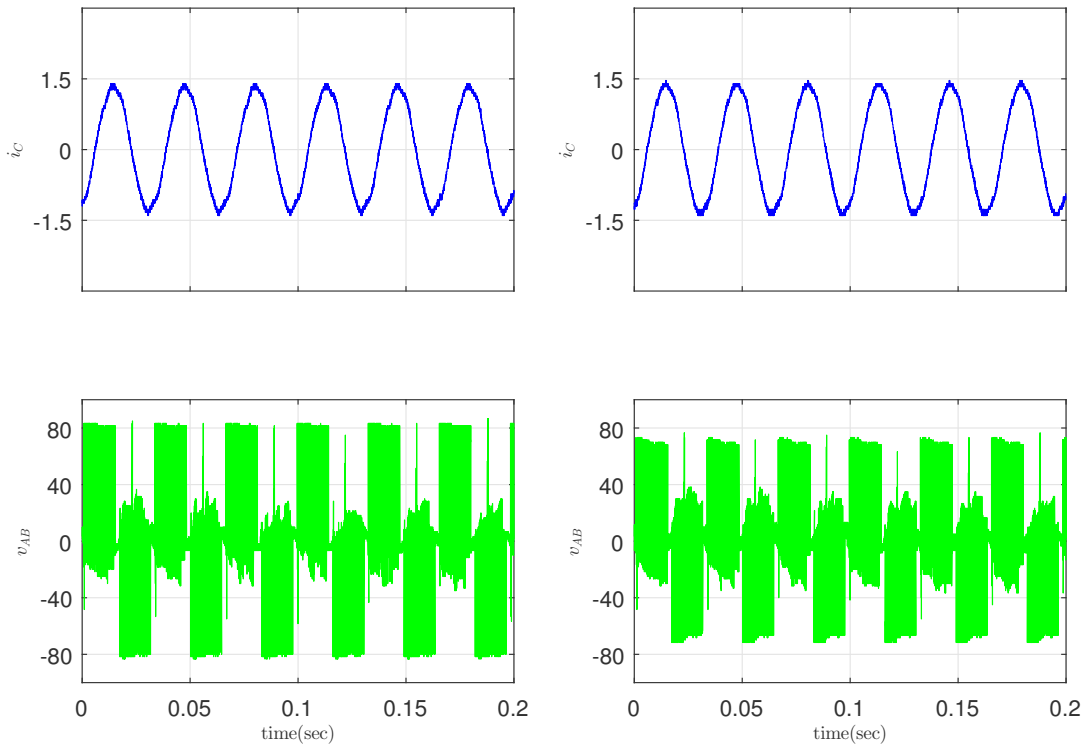

Figure 3.14: (a) Outputs when m_{v_H}=1 (b) Outputs with reduced m_{v_H}

3.7 Converter operation using a multilevel converter

The H Bridge topology was used in the generation of high frequency AC voltage from the DC source. The SHE modulation strategy was used and resulted in the generation of a switched voltage that switches between $+V_{dc}$ and 0 levels during the positive half cycle and switches between the $-V_{dc}$ and 0 levels in the negative half cycle. Using this topology, the conversion is accomplished by employing four semiconductor devices which have to switch multiple times in one fundamental cycle of the link voltage. The SHEPWM strategy was primarily chosen to eliminate lower harmonics in $v_{switched}$ so as to minimize any circulating currents into the LC tank. This can also be accomplished by using a regular PWM strategy and using a high switching frequency. At large voltage magnitudes of V_{dc}, the switching losses can be significant and the resulting $\frac{dv}{dt}$ across the transformer primary winding can be too high.

A multilevel converter can be used in place of the H Bridge to generate the high frequency AC link. Multilevel converters offer several advantages such as the generation of stepped output voltage with low THD, reduced $\frac{dv}{dt}$ and improved reliability. A high frequency AC link converter using a 9 level cascaded topology is shown in Fig. 3.15 . In recent times, modular multilevel converters(MMC) have been investigated and offer more benefits compared to the conventional multilevel topologies. A high frequency AC link converter using a MMC is shown in Fig. 3.15.

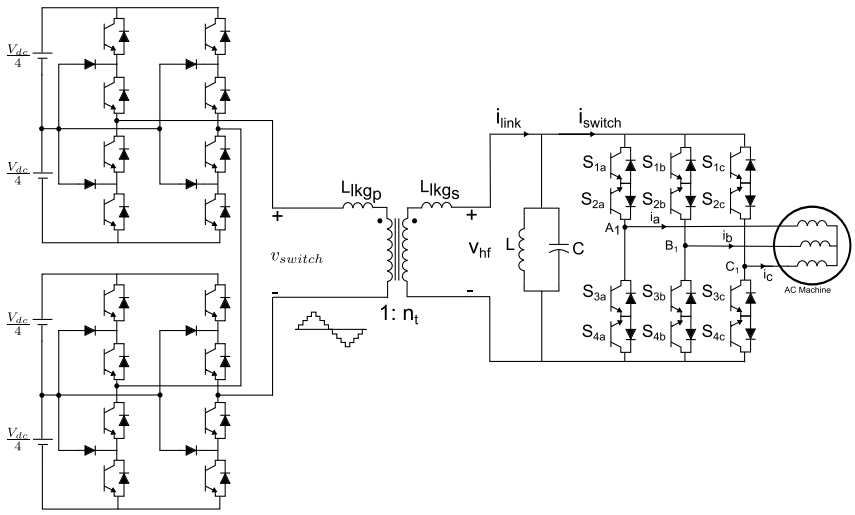

Figure 3.15: AC Link generation using Multilevel Converter

The operation with a cascaded multilevel converter needs four isolated DC sources as shown. These sources could be assumed to be four isolated PV strings or four individual batteries. The multilevel converter is modulated to generate a 9 level stepped output with the fundamental frequency of f_{hf}. Phase shifted carriers are used to generate the switching signals and the frequency of each of those carriers is the same as f_{hf} to generate the stepped waveform. The figure 3.16 shows the generation of a high frequency AC link using the previously mentioned SHEPWM and a multilevel stepped waveform.

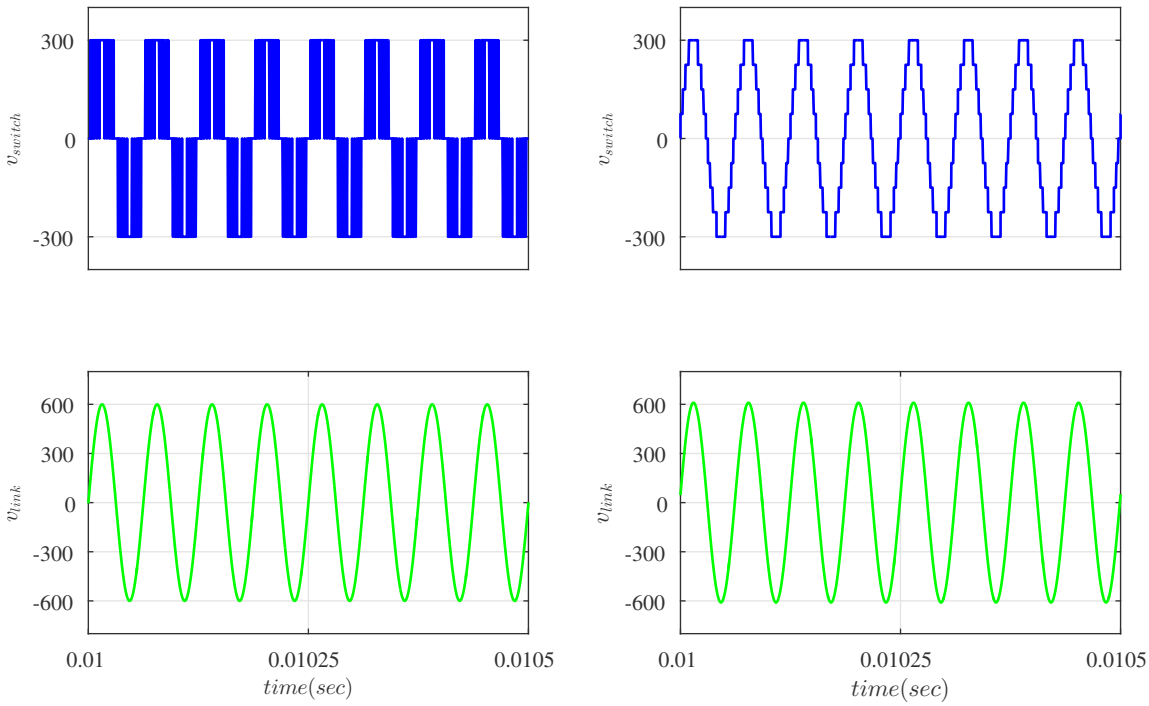

Figure 3.16: AC Link generation using H Bridge and Multilevel Converter

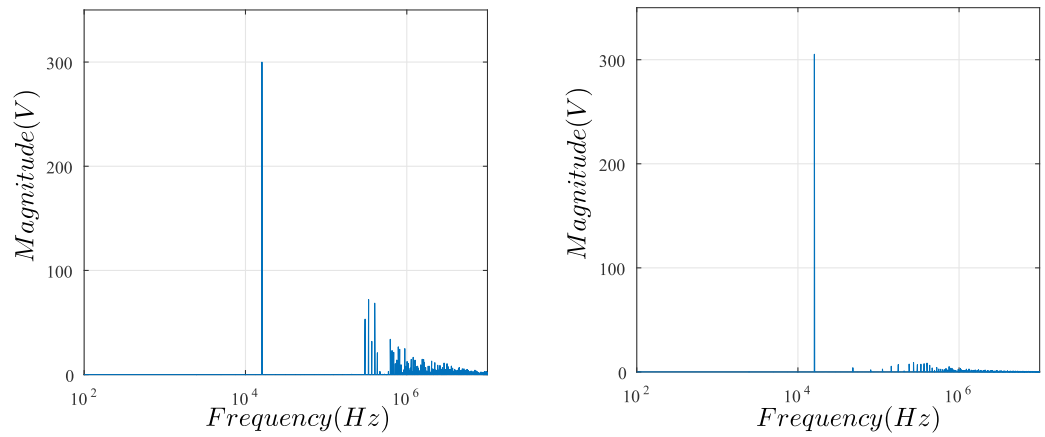

(a) (b)

Figure 3.17: (a) FFT of the voltage generated by H Bridge using SHE PWM (b) FFT of the voltage generated by 9 level multilevel converter

3.8 Summary

This chapter described a novel transformer isolated drive configuration which incorporates the benefits of high frequency ac link inverters and open end drives. Single stage conversion is achieved without the problem of leakage energy commutation by the use of the parallel resonant tank. Further, zero voltage switching is achieved in the cycloconverters which results in improved efficiency. Circulating currents in the open end windings are avoided by utilizing voltage vectors possessing the same common mode voltage to synthesize the output voltages. Moreover, the open end configuration leads to a higher overall voltage gain and the high frequency nature of the link yields a compact configuration with increased power density. The sinusoidal current through the transformer is advantageous as it avoids additional conduction losses that would have resulted from the harmonics in a square waveform. An alternate control scheme was proposed for controlling the magnitude of output voltages. The use of a multi-level converter to generate the high frequency link was also explained. Results from computer simulations and the hardware prototype are in agreement.

Chapter 4

High Frequency Link Inverter using a Partially Resonant Leg

4.1 Introduction

The previous chapters have explained how leakage commutation can be achieved by using a resonant LC circuit. As explained, the problem with the leakage inductance only arises when the current i_{switch} reverses in polarity. The earlier approach avoided fast changing currents by providing a low impedance path for the higher frequency harmonics in i_{switch} through the parallel tank. During operation, the tank has currents that continuously circulate between L_p and $C_p$which can lead to power losses due to winding resistance in the inductor. In this chapter, a new commutation technique is proposed where the rate of change of the current at the instant of cylcoconverter switching is controlled by a separate leg and that results in a resonant transition[1] . It is shown that by the addition of a separate leg comprising of a capacitor and a bidirectional switch, the problem of leakage energy commutation is overcome and soft switching is achieved.

[1] Parts of this chapter are taken from [71]

4.2 Description of the Converter

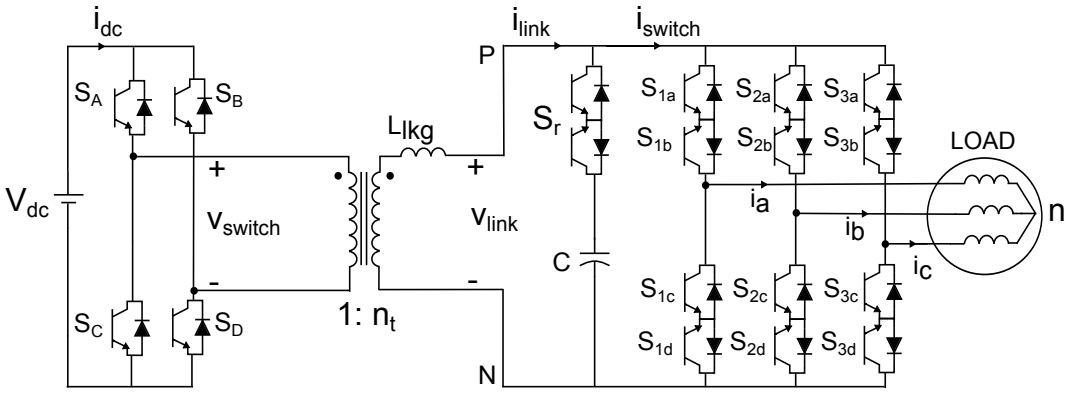

Figure 4.1: High frequency ac link inverter

The proposed high frequency ac link inverter is shown in Fig 4.1. It consists of an H-bridge comprising of switches S_A through S_D that is used to generate a high frequency square wave voltage from a DC voltage source unlike the previous chapters where the H-bridge was generating a PWM voltage. Turning on S_A and S_D leads to a positive link voltage across the transformer while turning on the switches S_B and S_C leads to a negative voltage. A high frequency transformer with a turns ratio of n_t is embedded in the link and L_{lkg} is the equivalent leakage inductance of this transformer referred to the secondary winding.

A cycloconverter consisting of switches S_{1a} through S_{3d} is connected across the secondary winding to synthesize the desired voltages of variable frequency and magnitude directly from the high frequency ac link voltage.The switches in a leg can be divided into positive and negative groups with S_{xa},S_{xb} belonging to the positive group and S_{xc},S_{xd} belonging to the negative group and x=1,2,3. An additional leg comprising of a capacitor C and a bidirectional switch S_r is connected across the secondary winding to facilitate a resonant transitions in the current through the transformer. The switch S_r is controlled to conduct only during those instants when the link current has to change its polarity.

The cycloconverter is modulated using the space vector modulation algorithm. Fig 4.2a depicts the six possible voltage vectors V_1 through V_6 and their associated switch

combination for a regular voltage source inverter. Additionally, two zero voltage vectors are possible using the switch combinations of [000] or [111]. The desired voltage space vector,$\overrightarrow{V_s}$, is synthesized on an average over a fixed sampling time by applying a combination of adjacent active vectors for specific time durations and a zero vector for the remainder of this time.In the space vector diagram shown in Fig 4.2a, the active voltage vector V1 is obtained by applying a switch combination of [100] meaning the positive group comprising of S_{1a}, S_{1b} in leg belonging to phase a is on while the negative group consisting of S_{2c}, S_{2d} and S_{3c}, S_{3d} is on in the legs belonging to phase b and c and so on. The switch combination of the three cycloconverter legs must be changed every time the link voltage changes its polarity [37] as shown in Fig 4.2b which consequently can cause the current i_{link} to abruptly reverse in polarity. If this current is allowed to flow through the transformer leakage inductance, it results in large overvoltages that can damage the switches or the transformer winding insulation. This chapter proposes a commutation technique that facilitates switching the cycloconverter without the problem of large overvoltages and recovers the energy trapped in the leakage inductance.

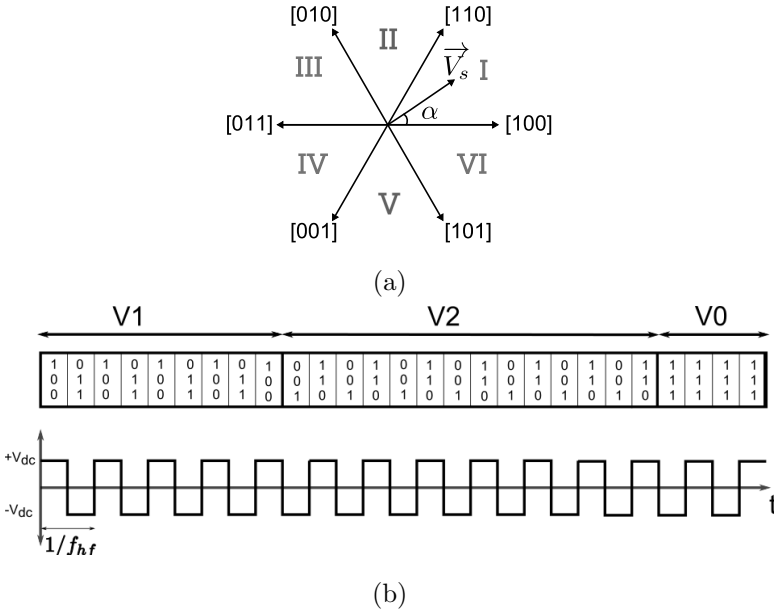

Figure 4.2: (a) Spacevector modulation (b) Switching scheme over one sampling period in Sector 1 and the associated link voltage

4.3 Description of the Commutation Process

As described in the previous section, the cyclconverter legs need to change their switching state each time the link voltage changes its polarity. During this switching process, it must be ensured that there is always a conducting path for the link current and the output currents. In this modulation scheme, it is assumed that the transformer link current changes polarity during majority of the cycloconverter state transitions.

4.3.1 Natural and Forced Commutation

The process of switching a power pole consisting of bidirectional switches is considered in this section. In a conventional configuration with a stiff DC bus, the power pole consists of two devices which are switched alternately with a small dead time between them. A suitable dead time is necessary to ensure that the the top and bottom devices do not conduct at the same time. During the dead time, the current flows through an anti-parallel diode that is present in parallel with the devices. However, the same technique cannot be used for switching a power pole comprising of bidirectional switches. If a dead time were to be introduced during the turn on or turn off instants, there will be no path for the power pole current to flow. The majority of the loads are inductive in nature and such an interruption in their currents is undesirable.

A technique that can be used to switch a bidirectional power pole is the four step commutation process. As the name suggests, the turn on or the turn off process is accomplished in four discrete steps. This process ensures that there is no interruption of the inductive load current while also guaranteeing that the power pole is not shorted. Information about the direction of the power pole current is needed to implement four step commutation. The following figures demonstrate the turn off switching process for all polarities of bus voltage and power pole current. It can be seen that the first step is to turn off the switch through which no current is flowing. As a second step, the switch which will conduct the current, depending on the polarity of the current, is turned on. This switch will be called as the active incoming switch. In the third step, the switch through which current was initally flowing is turned off and this switch is referred to as the outgoing active switch. In the final step, the remaining switch in the incoming bidirectional pair is turned on.

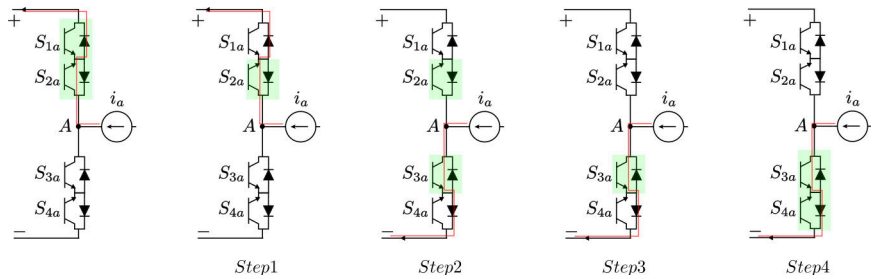

Figure 4.3: Positive voltage, negative current

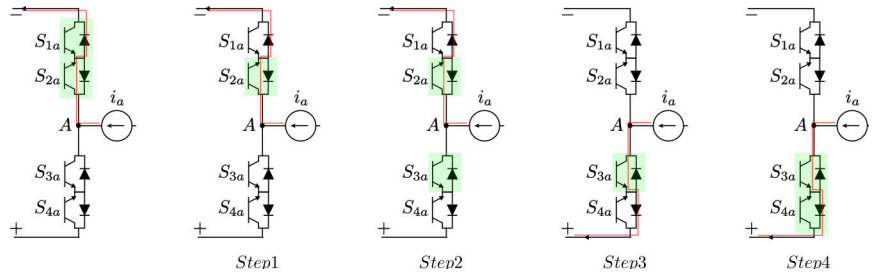

Figure 4.4: Negative voltage, Negative current

It can be seen that the transfer of current can happen in either the second or the third steps depending on the voltage and current polarities. If the current transfer occurs in the second step i.e when the incoming active switch is gated on, such a type of current transfer is called natural commutation of leg current. On the other hand, if the current transfer only occurs when the active outgoing switch is turn off in the third step, it is called forced commutation of leg current.

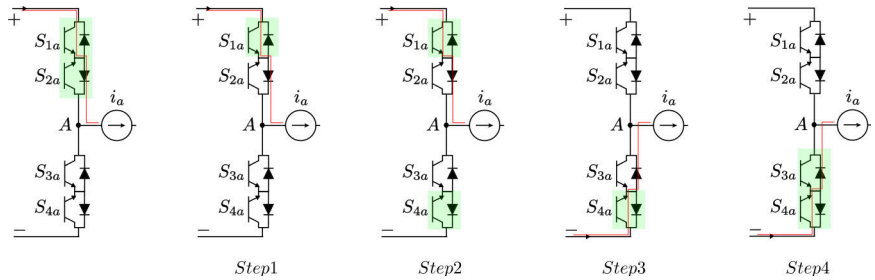

Figure 4.5: Positive voltage, positive current

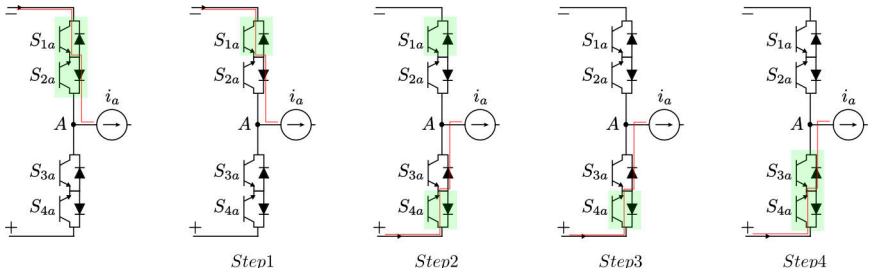

Figure 4.6: Negative voltage, positive current

It can be seen from Fig. 4.2b that there exist two modes which dictate the final value of the link current when a switching transition happens in the cycloconverter. When a given active vector,V_1 or V_2 or V_0 is being applied, all three legs need to change their state when the link voltage polarity changes. In this case, the magnitude of the link current remains the same but the polarity reverses.This switching process is explained in subsection 4.3.2.The switching process during the transition from one active vector to the next active vector utilizes a 'shoot through' state and is described in subsection 4.3.3. During this type of transition, the current applied by the cycloconverter on the ac link is different in magnitude and will have the opposite polarity. The switching process during those instants when the link current does not change in polarity is described in subsection 4.3.4.

A flowchart describing the general sequence of switching states is presented in Fig. 4.8. The switch group that is being turned off is called the outgoing group while the group that is being turned on is the incoming group. The switch which is conducting current is referred to as the active switch while the non-conducting switch is called the passive switch. The actual current transfer from the outgoing switch to the incoming switch is decided by whether the current commutation process for a leg is natural or forced as described in [72]. It can be seen from this chart that the switching of the H-Bridge can occur either at the beginning of process or towards the end of the process depending on the kind of transition taking place.

To explain the switching process, assume that the desired space vector is located in Sector 1. It is synthesized by applying the active voltage vectors V1, V2 and a zero vector. The load is modeled as a balanced three phase current source, the magnetizing inductance of the transformer is assumed to be large and the winding resistance is

neglected.

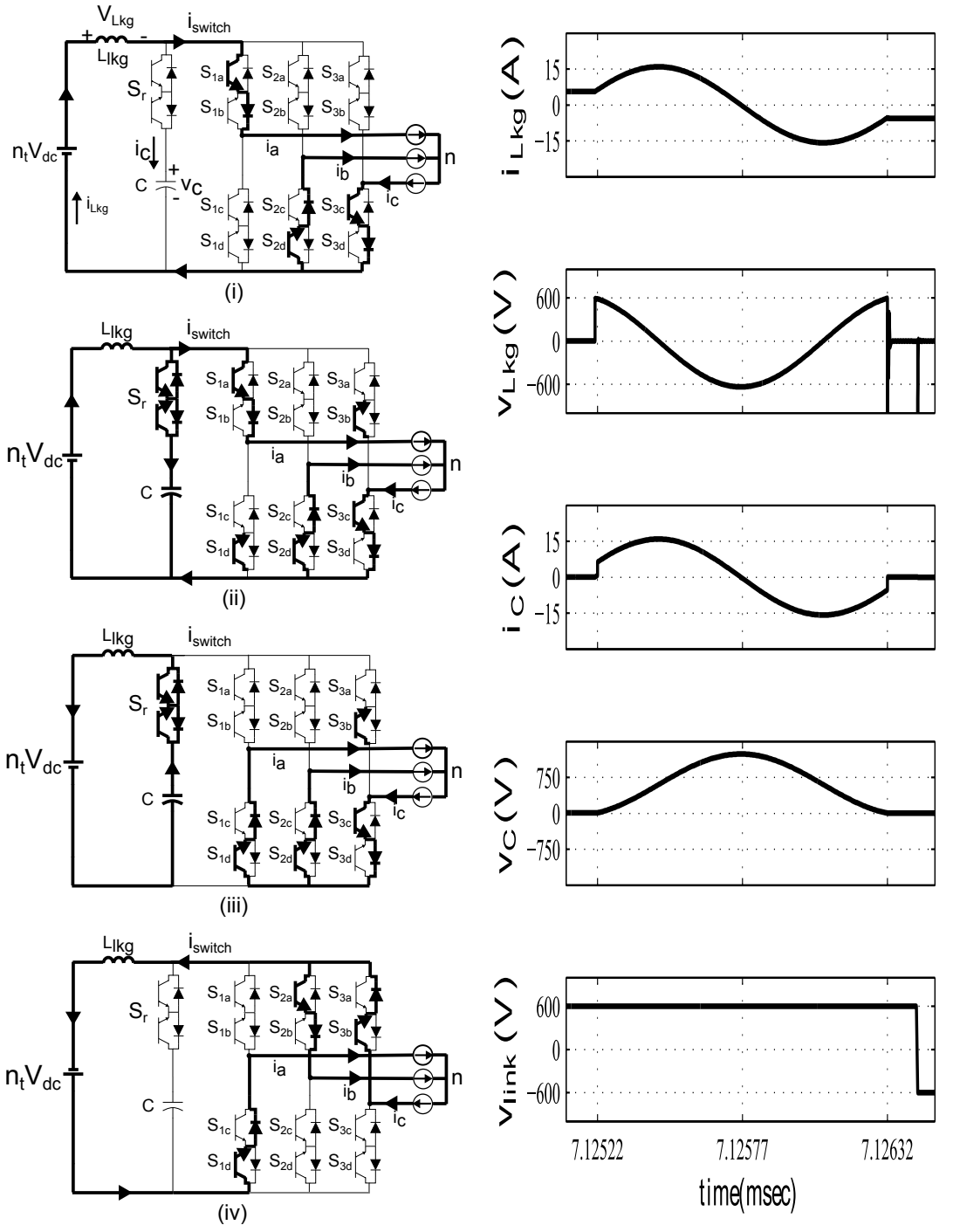

(a) (b)

Figure 4.7: (a) Switching when applying a single vector (b) Top to Bottom: Current and voltages of the leakage inductance and capacitor and link voltage

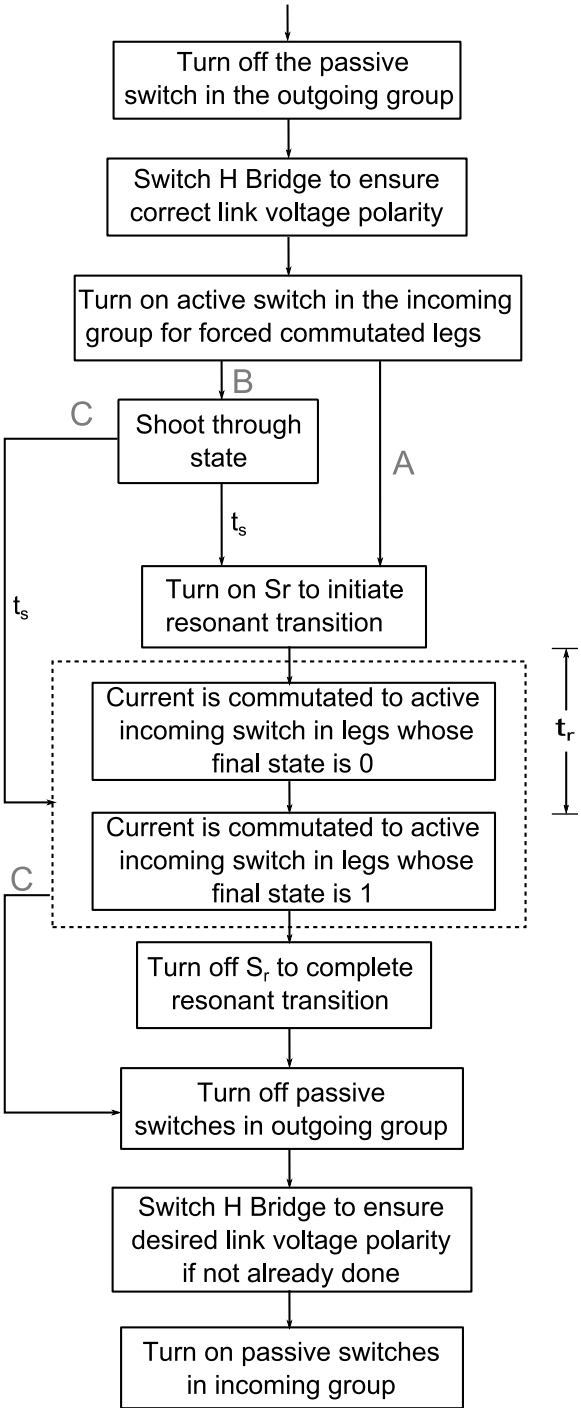

Figure 4.8: Commutation steps in the proposed technique

4.3.2 Switching when applying a voltage vector

Without loss of generality, assume that the active vector V1 is being applied and the link voltage is positive. The current flowing through the leakage inductance, i_{Lkg}, equals the current i_a in this state. When the link voltage goes negative, the switch state of each leg needs to be inverted i.e the new switch combination to be applied is [011]. In this transition, all the three legs of the cycloconverter change their state. The switches in phase a need to make a transition from 1 to 0 while switches in phase b and c need to make a transition from 0 to 1. Considering the three phase load currents to be balanced, the link current in this new switch state will now be $-i_a$. The output current can be approximated as a DC quantity with a magnitude of say 'I' for this transition. The initial voltage on the capacitor C is zero volts. The equivalent circuit of the converter under these assumptions is shown in Fig. 4.7a and this process is shown as 'A' in the flowchart of Fig. 4.8. The process of switching from [100] to [011] is described as follows :

1. As a first step, the passive switches among the currently on switches are turned off . This means switches S_{1b}, S_{2c} and S_{3d} are turned off without affecting the flow of current and this is shown in circuit (i) of Fig. 4.7a. The turn off of these switches is a zero current switching(ZCS) and hence there is no switching loss associated with this transition.

2. In this step, the H-Bridge is switched such that the link voltage has the same polarity as the link current which is assumed positive in this discussion. Since the link voltage is initially assumed positive, there is no change of state of the H-Bridge in this step.

3. The switches S_{1d} and S_{3b} are gated on as seen in the second circuit of Fig. 4.7a as they will conduct current in the next switch state and undergo forced commutation .Since these switches are reverse biased, there is no change in the current path through the converter legs. It can be seen that the turning on of all the switches in this step takes place under ZCS conditions.

4. In this step, the switch S_r is turned on initiating the resonant transition.

5. Once the switch S_r is turned on, current is transferred to the negative group in legs with final state as 0. This ensures that the load current free wheels in the bottom group. The switch S_{1a} is turned off after a short time and the current in leg belonging to phase a now shifts to S_{1d}. The current i_{link} flows through the capacitor. Since the capacitor voltage is close to zero, the turn off of switch S_{1a} results in a low switching loss.

6. In this step, the current in the leakage inductance resonates with the capacitor as illustrated in the circuit (iii) of Fig. 4.7a. This resonance is allowed until the current in the inductance reaches the value -I and simultaneously, the capacitor voltage now returns back to its initial voltage of zero volts. The inductor current during resonance is given by (4.1) and the time required by the current to reach -I is given by (4.3). The capacitor voltage during this interval is given by (4.2).

$$i_{Lkg}(t) = \sqrt{\frac{(n_t V_{dc})^2 C}{L_{Lkg}} + I^2}\sin(\omega_n t + \Phi) \tag{4.1}$$

$$v_C(t) = n_t V_d c - \sqrt{(n_t V_{dc})^2 + \frac{(I L_{Lkg})^2}{C}}\cos(\omega_n t + \Phi) \tag{4.2}$$

where, $\omega_n = \dfrac{1}{\sqrt{L_{Lkg}C}}$, $\Phi = \arctan\dfrac{I L_{Lkg}\omega_n}{n_t V_{dc}}$

$$t_r = 2\frac{\pi - \Phi}{\omega_n} \tag{4.3}$$

7. At the end of the resonant interval, current is transferred to the positive group in the legs whose final state is 1. Turning on the switch S_{2b} causes the current to transfer from switch S_{2c} whereas the current is transferred to the already gated on switch S_{3b} by turning off S_{3c}.

8. The switch S_r is turned off while the H-bridge is now switched to generate negative voltage as shown in circuit (iv) of Fig. 4.7a. Switches S_{2c} and S_{3c} can now be turned off under ZCS conditions. The switching process is complete when the switches S_{1c}, S_{2b} and S_{3a} are turned on under zero voltage switching(ZVS) conditions.

4.3.3 Switching to a different active vector

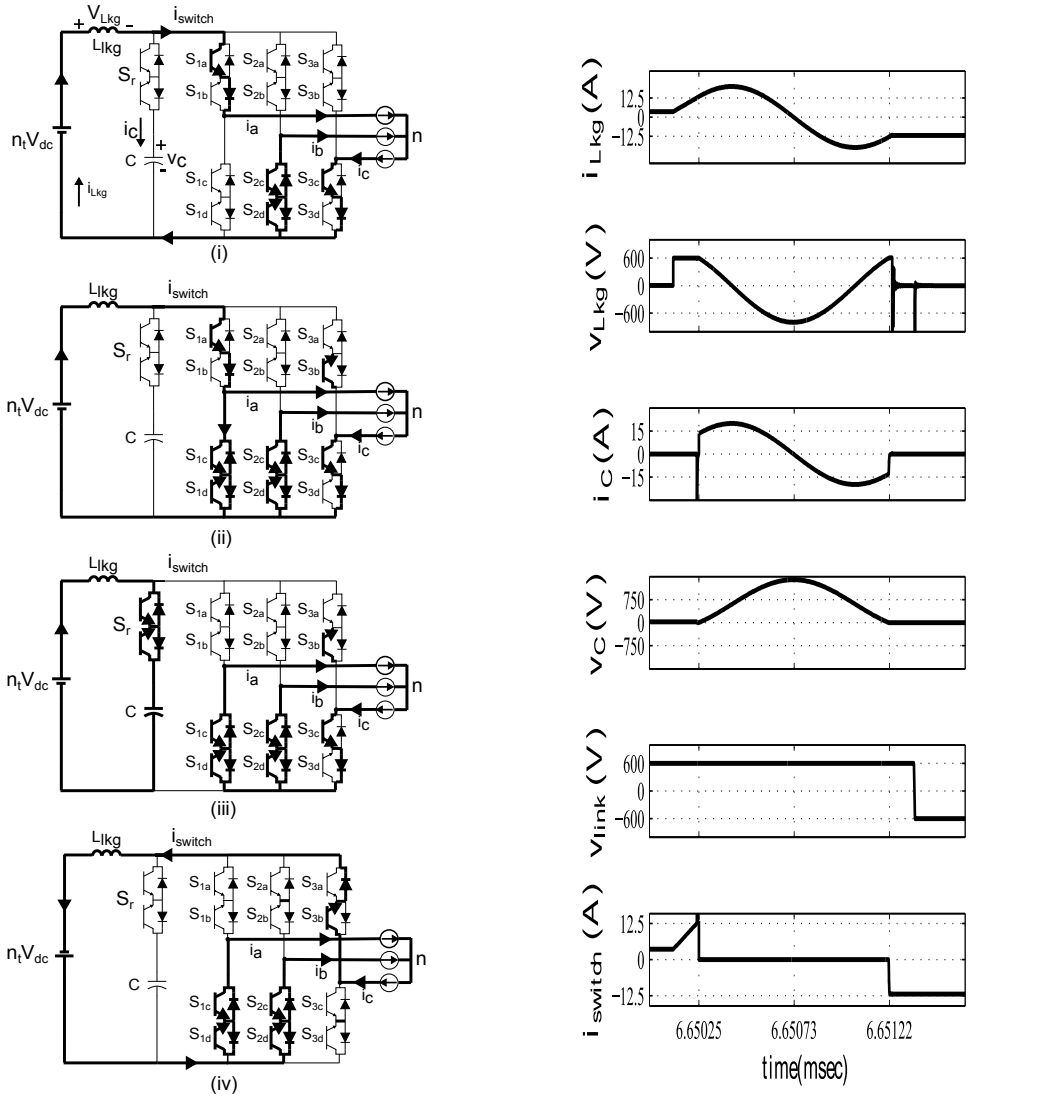

Figure 4.9: (a) Commutation when transitioning to a different active vector (b) Top to Bottom: Current and voltages of leakage inductance and capacitor, link voltage and input current of cycloconverter during transition to a different active vector

Assume that the initial state of the circuit is the same as previously assumed and now, the active vector V2 needs to be applied. Also assume without loss of generality that the link current has a magnitude I which is less than the current that results on application of V2, say I $+\Delta I$. Since the link voltage polarity will be negative, the switch configuration [001] will need to be applied as can be observed from Fig. 4.2b. When transitioning between adjacent active vectors, only two legs will change their state. It can be seen that phase b retains its switch state of 0 and so need not be switched. A shoot through state is introduced during which the leg belonging to phase a is deliberately shorted to change the link current in the leakage inductance to a desired value. The steps involved in this process are identical to the previous transition except for an additional shoot through state. The sequence of steps is observed from Fig. 4.8 where the path marked 'B' shows that an additional shoot through state is necessary.

During the shoot through state, the current in the link inductor is increased by ΔI by turning on switch S_{1c} and deliberately shorting the leg as shown in circuit (ii) of Fig. 4.9a. The time for this transition is given by (4.4)

$$t_s = L_{lkg}\frac{\Delta I}{n_t V_{dc}} \tag{4.4}$$

Once the current in the leakage inductance builds up to the desired value, the switch S_r is turned on and switch S_{1a} is turned off after a short duration with the low capacitor voltage across it. The current in leg of phase a now transfers to the switch S_{1d} which was already gated on. The current in the leakage inductance, which now has the value $I + \Delta I$, resonates with the capacitor as shown in circuit (iii) of Fig. 4.9a. The current is allowed to resonate for time t_r given by (4.3) when it has the magnitude -($I + \Delta I$) and the capacitor voltage simultaneously returns to its initial value of zero volts.

4.3.4 Switching to a different active vector without change of link current polarity

It is possible that the link current does not change in polarity when the next active vector is applied. In such a case, the switch S_r is not used and no resonance occurs. The steps in this process can be observed from Fig. 4.8 where the arrow marked 'C' denotes the path during this transition. Once the shoot through state is completed after

time t_s, the current transfer from the outgoing to the incoming switch in all legs takes place in the same step as denoted by the larger box with dashed lines.

4.4 Capacitor Sizing

The appropriate capacitor value is decided by utilizing the following design equations. The leakage inductance of the transformer is assumed to be known and is equal to L_{lkg}. The value of the capacitor affects the time taken for the reversal of link current and ideally, this time should be kept as small as possible. The time for the resonant transition, t_r is given by (4.3) and it can be observed that a smaller valued capacitor leads to faster current reversal.

However, it can be observed from (4.1) and (4.2) that the peak values of the capacitor current and voltage during the resonant transition depend on the value of the capacitor. A decrease in the resonant time interval is accompanied by a corresponding increase in the peak voltage across the link and the consequent increase in the voltage rating of switches used in the cycloconverter. The time for current reversal also affects the output voltage as it can be seen from Fig 4.7a that there is no output voltage during this period.

A parameter X is defined as the ratio of the maximum resonant time interval and half the time period of the link voltage as shown in (4.5).

$$X = \frac{t_r}{2T_{hf}} \tag{4.5}$$

To calculate the appropriate value of X, a converter supplying a 10kW load with a power factor of 0.8 was assumed. The line line rms voltage is 415V. A leakage inductance of 8 μH and a link frequency f_{hf} of 20 kHz was assumed. Moreover, it is assumed that V_{dc}=600V and n_t=1. The peak values of the capacitor current and voltage are given by (4.6) and (4.7) and occur when the link current, I equals the peak value of the output current

$$\hat{I}_c = \sqrt{\frac{(n_t V_{dc})^2 C}{L_{Lkg}} + I^2} \tag{4.6}$$

$$\hat{V}_c = n_t V_d c + \sqrt{(n_t V_{dc})^2 + \frac{(IL_{Lkg})^2}{C}} \tag{4.7}$$

A graph showing the variation of the ratio of peak capacitor current to the peak load current and ratio of peak capacitor voltage to the link voltage as a function of X(in percent) is shown in Fig. 4.10. Choosing the value of X as 10% results in capacitor of 19.78 nF while $\hat{I}_c$=1.6 and $\hat{V}_c$=2.3.

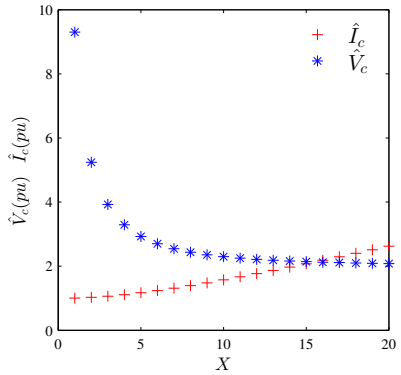

Figure 4.10: Variation of peak capacitor voltage and current with X

4.5 Simulation Results

The commutation technique described was simulated in the SIMULINK environment. The first plot of Fig. 4.7b shows the resonant transition of i_{Lkg} when applying an active vector. Fig. 4.9b shows the waveforms when switching to a different active vector. The sixth plot shows the current i_{switch} linearly changing during the shoot through state and the plot of v_{Lkg} has a constant voltage during this time. Fig. 4.11a shows the link current and link voltage on a larger time scale. Fig. 4.11b shows the capacitor current and voltage and it can be seen that v_c returns to zero voltage after every transition. The switched nature of the output phase voltage is shown in Fig. 4.12 and it can be observed that this voltage periodically goes to zero corresponding to the resonant current reversals.

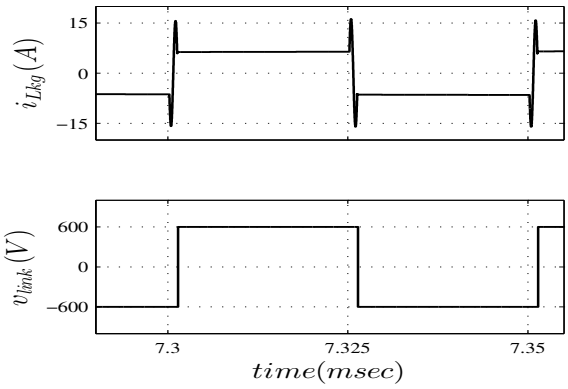

(a)

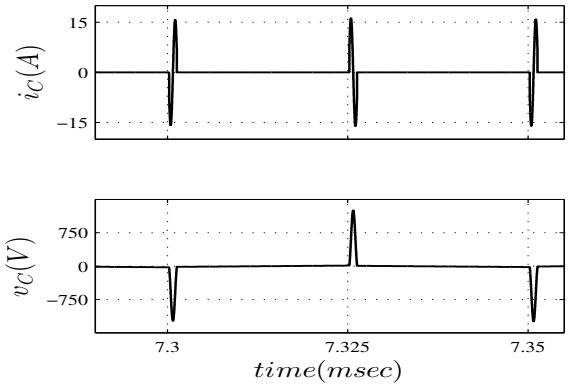

(b)

Figure 4.11: (a) Current through leakage inductance and voltage across link in steady state (b) Capacitor current and voltage in steady state

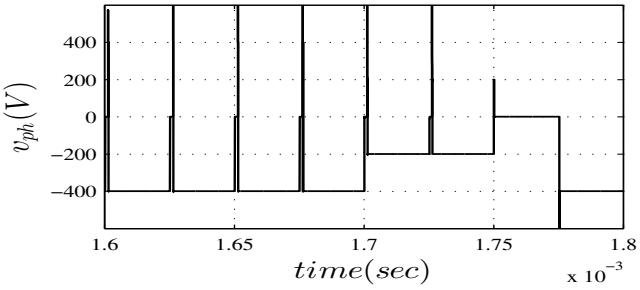

Figure 4.12: Switched phase voltage over one sampling period

4.6 Summary

A technique to safely commutate the energy trapped in the leakage inductance of the transformer is presented. The resonant transfer of current to the opposite polarity during switching transitions also causes majority of the switch transitions to be soft switched resulting in reduced switch losses, lower heat dissipation and a compact overall design. Bidirectional power flow is also possible when using this technique. Despite the advantages, this scheme needs the use of current sensors to monitor the output currents and the link current. It also needs a careful design of the capacitor to avoid increased device stresses during the resonant transitions. A voltage clamp circuit might still be needed as even a small mismatch of currents after the resonant interval can lead to a voltage spike. However, compared to a circuit configuration where there is no proper scheme to commutate the trapped leakage energy, the energy dissipated in the clamp circuit will be very low.

Chapter 5

Conclusion and Future Work

The thesis discussed two configurations of high frequency AC link inverters which avoid the problem of leakage energy commutation. The first idea was to use a resonant tank across the cycloconverter and the tank offers low impedance path for the high frequency harmonics of i_{switch}. Thus, the resulting current flowing through the leakage inductance of the transformer is devoid of abrupt changes in current. A discrete space vector modulation technique was presented that can be used to synthesize balanced three phase voltages from the sinusoidal link. Switching losses in the cycloconverter are eliminated by only changing the switch states near the zero crossing regions. This idea was extended to operate an induction motor in an open end configuration and the open end configuration increases the overall gain of the converter. The stress on the motor windings is low due to the application of sinusoidal half cycles and the absence of large $\frac{dv}{dt}$ at the motor terminals. The common mode voltage was found to be primarily concentrated at the link frequency and does not lead to adverse bearing currents. The second idea presented the use of an additional leg across the cycloconverter to result in sinusoidal resonant transitions in the link currents. By carefully timing the switching signals of the switches, it was shown that the additional leg only needs to operate for a very short interval and also results in regions of zero voltage.

By using these approaches, it can be concluded that the leakage inductance of the transformer does not pose any difficulties when used in single stage high frequency AC link topologies. This reduces the need to maintain the leakage inductance at a minimum value when designing the transformer. In fact, when using the additional

leg to achieve resonant current transitions, the circuit relies on the leakage inductance to achieve resonance. The need for dissipative clamp circuits is avoided and the high frequency nature of the link results in a compact sizes of the transformer and inductor.

Although both the approaches are successful in mitigating the problem posed by the leakage energy, they use two completely different approaches which present their own unique challenges. The first approach has large circulating currents flowing through the tank comprised of passive components. In practice, an inductor always exhibits a finite winding resistance and the resistance increases with the operating frequency. Thus, to achieve a large power conversion efficiency, the inductor has to be carefully designed to reduce the winding resistance. The conversion gain for the single ended inverter using the resonant LC tank is shown to be 0.3675. This is lower than the 0.577 gain of an inverter that operates using a space vector modulated DC bus. This means that the peak value of the link voltage needs to be higher to meet the voltage generation capability of the DC bus based voltage source inverter. The transformer turns ratio can be easily adjusted to obtain the desired value of the link voltage but the need for a higher peak voltage requires the use of devices with larger voltage ratings in the cycloconverter.

The use of the additional leg to achieve resonant transitions in the link current does not rely on continuous resonance. Instead, the resonant period is only a small fraction of the link frequency. However, during these resonant intervals, the output voltage is zero and the final output voltage will be slightly lower. This drawback can be overcome by using a closed loop control strategy to ensure that the desired voltages are being generated or by using a larger magnitude of the AC link voltage. The loss in the output voltage can be reduced by shortening the resonant interval but this increases the peak value of the voltage across the resonant capacitor. Thus, there exists a tradeoff between loss of output voltage and peak voltage stress during the resonant interval. The operation of this approach also relies on the accurate timing of the gate pulses and it is therefore important to accurately characterize any delays in the gate drive circuits.

The contributions of this thesis open up several possibilities for further research some of which are :

- The proposed schemes can be compared with two stage power conversion approaches (such as using a high frequency transformer isolated Dual Active Bridge topology) and demonstrate the advantages of single stage conversion

- Designs of high frequency inductors capable of carrying high current and having low winding resistance can be investigated the resonant LC tank
- The effect of finite device resistances on the operation of partially resonant additional leg needs to be analyzed and its effect on the capacitor voltage needs to established.
- The output filter size for inverters using a sinusoidal AC link can be compared with the filter size of a traditional DC bus based inverter.
- The proposed ideas can be extended to AC-AC converters and their benefits can be explored.

References

[1] David Appleyard. Global renewable energy is status positive. http://www.renewableenergyworld.com/articles/2015/07/global-renewable-energy-is-status-positive.html.

[2] F. Blaabjerg, F. Iov, R. Teodorescu, and Z. Chen. Power Electronics in Renewable Energy Systems. *2006 12th International Power Electronics and Motion Control Conference*, pages 1–17, aug 2006.

[3] Office of Energy Efficiency and Renewable Energy. http://energy.gov/eere/sunshot/power-electronics.

[4] Jay M. Erdman, Russel J. Kerkman, David W. Schlegel, and Gary L. Skibinski. Effect of PWM inverters on ac motor bearing currents and shaft voltages. *IEEE Transactions on Industry Applications*, 32(2):250–259, 1996.

[5] Huai Wang, Marco Liserre, and Frede Blaabjerg. Toward reliable power electronics: Challenges, design tools, and opportunities. *IEEE Industrial Electronics Magazine*, 7(2):17–26, 2013.

[6] C. M. D. O. Stein, H. A. Grundlong, H. Pinheiro, J. R. Pinheiro, and H. L. Hey. Analysis and comparison of soft-transition inverters. In *Industrial Electronics, 2003. ISIE '03. 2003 IEEE International Symposium on*, volume 1, pages 538–543 vol. 1, June 2003.

[7] Maria D. Bellar, Tzong Shiann Wu, Aristide Tchamdjou, Javad Mahdavi, and M. Ehsani. A review of soft-switched DC-AC converters. *IEEE Transactions on Industry Applications*, 34(4):847–860, 1998.

[8] R.W. De Doncker and J.P. Lyons. The auxiliary resonant commutated pole converter. *Conference Record of the 1990 IEEE Industry Applications Society Annual Meeting*, pages 1228–1235, 1990.

[9] Deepakraj M. Divan. The Resonant DC Link Converter-A New Concept in Static Power Conversion. *IEEE Transactions on Industry Applications*, 25(2):317–325, 1989.

[10] Deepakraj M Divan and Gary Skibinski. Zero-switching-loss inverters for high-power applications. *Industry Applications, IEEE Transactions on*, 25(4):634–643, 1989.

[11] R W De Doncker, J.P. P Lyons, R.W. De Doncker, and J.P. P Lyons. The auxiliary quasi-resonant DC link inverter. *PESC '91 Record 22nd Annual IEEE Power Electronics Specialists Conference*, pages 248–253, 1991.

[12] B. Zhao, Q. Song, and W. Liu. A practical solution of high-frequency-link bidirectional solid-state transformer based on advanced components in hybrid microgrid. *IEEE Transactions on Industrial Electronics*, 62(7):4587–4597, July 2015.

[13] A. K. Jain and R. Ayyanar. Pwm control of dual active bridge: Comprehensive analysis and experimental verification. *IEEE Transactions on Power Electronics*, 26(4):1215–1227, April 2011.

[14] Bo Yang, F. C. Lee, A. J. Zhang, and Guisong Huang. Llc resonant converter for front end dc/dc conversion. In *Applied Power Electronics Conference and Exposition, 2002. APEC 2002. Seventeenth Annual IEEE*, volume 2, pages 1108–1112 vol.2, 2002.

[15] A. Hillers, D. Christen, and J. Biela. Design of a highly efficient bidirectional isolated llc resonant converter. In *Power Electronics and Motion Control Conference (EPE/PEMC), 2012 15th International*, pages DS2b.13–1–DS2b.13–8, Sept 2012.

[16] William McMurray. The Thyristor Electronic Transformer: a Power Converter Using a High-Frequency Link. *IEEE Transactions on Industry and General Applications*, IGA-7(4):451–457, 1971.

[17] W. McMurray. A constant turn-off time control for variable frequency thyristor inverters. *IEEE Transactions on Industry Applications*, IA-13(5):418–422, Sept 1977.

[18] Paul M. Espelage and Bimal K. Bose. High-Frequency Link Power Conversion. *IEEE Transactions on Industry Applications*, IA-13(5):387–394, sep 1977.

[19] V. T. Ranganathan, Phoivos D. Ziogas, and Victor R. Stefanovic. A DC-AC Power Conversion Technique Using Twin Resonant High-Frequency Links. *IEEE Transactions on Industry Applications*, IA-19(3):393–400, 1983.

[20] Ashoka K S Bhat and S. D. Dewan. Resonant inverters for photovoltaic array to utility interface. *IEEE Transactions on Aerospace and Electronic Systems*, 24(4):377–386, 1988.

[21] P.K. Sood and T.A. Lipo. Power conversion distribution system using a high-frequency ac link. *Industry Applications, IEEE Transactions on*, 24(2):288–300, 1988.

[22] P.K. Sood, T.A. Lipo, and I.G. Hansen. A versatile power converter for high-frequency link systems. *Power Electronics, IEEE Transactions on*, 3(4):383–390, 1988.

[23] K. Inagaki and S. Okuma. High frequency link dc/ac converters using three phase output pwm cycloconverters for uninterruptible power supplies. In *Telecommunications Energy Conference, 1991. INTELEC '91., 13th International*, pages 580–586, Nov 1991.

[24] Sudip K. Mazumder. Hybrid modulation scheme for a high-frequency AC-link inverter. *IEEE Transactions on Power Electronics*, 31(1):861–870, 2016.

[25] Deshang Sha and Jianliang Chen. Bidirectional three-phase high-frequency ac link dcac converter used for energy storage. *IET Power Electronics*, 8(12):2529–2536, 2015.

[26] Hamidreza Keyhani and Hamid A. Toliyat. Single-stage multistring PV inverter with an isolated high-frequency link and soft-switching operation. *IEEE Transactions on Power Electronics*, 29(8):3919–3929, 2014.

[27] Wenjie Zhu, Keliang Zhou, and Ming Cheng. A bidirectional high-frequency-link single-phase inverter: Modulation, modeling, and control. *IEEE Transactions on Power Electronics*, 29(8):4049–4057, 2014.

[28] Mahshid Amirabadi, Anand Balakrishnan, Hamid A. Toliyat, and William C. Alexander. High-frequency AC-link PV inverter. *IEEE Transactions on Industrial Electronics*, 61(1):281–291, 2014.

[29] Huai Wang and Frede Blaabjerg. Reliability of capacitors for DC-link applications in power electronic convertersan overview. *IEEE Transactions on Industry Applications*, 50(5):3569–3578, 2014.

[30] Michael Salcone and Joe Bond. Selecting film bus link capacitors for high performance inverter applications. *2009 IEEE International Electric Machines and Drives Conference, IEMDC '09*, pages 1692–1699, 2009.

[31] Huiqing Wen, Weidong Xiao, Xuhui Wen, and Peter Armstrong. Analysis and evaluation of DC-link capacitors for high-power-density electric vehicle drive systems. *IEEE Transactions on Vehicular Technology*, 61(7):2950–2964, 2012.

[32] Mustansir H Kheraluwala, Randal W Gascoigne, Deepakraj M Divan, and Eric D Baumann. Performance Characterization. *Ieee Transactions on Industry Applications*, 28(6):1294–1301, 1992.

[33] Rajapandian Ayyanar and Ned Mohan. Novel soft-switching DC-DC converter with full ZVS-range and reduced filter requirement - Part II: Constant-input, variable-output applications. *IEEE Transactions on Power Electronics*, 16(2):193–200, 2001.

[34] L Hui, B Ozpineci, and B K Bose. A soft-switched high frequency non-resonant link integral pulse modulated dc-ac converter for AC motor drive. *Iecon '98 - Proceedings of the 24th Annual Conference of the Ieee Industrial Electronics Society, Vols 1-4*, pages 726–732, 1998.

[35] K. Basu and M. Ned. A high frequency link single stage pwm inverter with common-mode voltage suppression and source based commutation of leakage energy. *Power Electronics, IEEE Transactions on*, PP(99):1–1, 2013.

[36] M. Matsui, M. Nagai, M. Mochizuki, and A. Nabae. High-frequency link dc/ac converter with suppressed voltage clamp circuits-naturally commutated phase angle control with self turn-off devices. *Industry Applications, IEEE Transactions on*, 32(2):293–300, 1996.

[37] I. Yamato and N. Tokunaga. Power loss reduction techniques for three phase high frequency link dc-ac converter. In *Power Electronics Specialists Conference, 1993. PESC '93 Record., 24th Annual IEEE*, pages 663–668, 1993.

[38] Shabari Nath and Ned Mohan. A solid sate power converter with sinusoidal currents in high frequency transformer for power system applications. *2011 IEEE International Conference on Industrial Technology*, pages 110–114, mar 2011.

[39] Shabari Nath and Ned Mohan. A matrix converter fed sinusoidal input output three winding high frequency transformer with zero common mode voltage. *2011 International Conference on Power Engineering, Energy and Electrical Drives*, (May):1–6, may 2011.

[40] Kartik V. Iyer and Ned Mohan. Multi-level converter to interface low voltage DC to 3-phase high voltage grid with medium frequency transformer isolation. *Proceedings, IECON 2014 - 40th Annual Conference of the IEEE Industrial Electronics Society*, pages 4683–4689, 2014.

[41] S.B. Kjaer, J.K. Pedersen, and F. Blaabjerg. A review of single-phase grid-connected inverters for photovoltaic modules. *Industry Applications, IEEE Transactions on*, 41(5):1292–1306, 2005.

[42] S.K. Mazumder, R.K. Burra, R. Huang, M. Tahir, K. Acharya, G. Garcia, S. Pro, O. Rodrigues, and M. Stasinopoulos. Single-stage low-cost and energy-efficient isolated phase-shifted high-frequency inverter followed by a forced cycloconverter for universal residential fuel cell power system. In *Electro/Information Technology, 2008. EIT 2008. IEEE International Conference on*, pages 408–413, 2008.

[43] Li Zhu, Keliang Zhou, Wenjie Zhu, and Xiu'E Su. High frequency link single-phase grid-connected PV inverter. *2nd International Symposium on Power Electronics for Distributed Generation Systems, PEDG 2010*, (2):133–137, 2010.

[44] Zainal Salam, Nge Chee Lim, Toh Leong Soon, and Mohd Zulkifli Ramli. Cycloconverter-Type High Frequency Link Inverter for Photovoltaic Application. 67(1):49–56, 2006.

[45] Mikihiko Matsui, Masaki Nagai, Masayuki Mochizuki, and Akira Nabae. High-frequency link dc/ac converter with suppressed voltage clamp circuits -naturally commutated phase angle control with self turn-off devices. *IEEE Transactions on Industry Applications*, 32(2):293–300, 1996.

[46] Takao Kawabata. High Frequency Link DC-AC Converter with PWM Cycloconverter. *Control*, 00(1), 1998.

[47] Li Hui, B. Ozpineci, and B.K. Bose. A soft-switched high frequency nonresonant link integral pulse modulated dc-ac converter for ac motor drive. In *Industrial Electronics Society, 1998. IECON '98. Proceedings of the 24th Annual Conference of the IEEE*, volume 2, pages 726–732 vol.2, 1998.

[48] Kaushik Basu and Ned Mohan. A High Frequency Link Single Stage PWM Inverter with Common-Mode Voltage Suppression and Source based Commutation of Leakage Energy. (c):1–12, 2013.

[49] Jose Juan Sandoval, Harish Krishnamoorthy, Prasad Enjeti, and Sewan Choi. High power density adjustable speed drive topology with medium frequency transformer isolation. *2015 IEEE Energy Conversion Congress and Exposition, ECCE 2015*, pages 6986–6992, 2015.

[50] Matrix converter fed power electronic transformer with enhanced features.

[51] S. Gandikota and N. Mohan. High frequency ac-link transformer isolated three phase inverter with natural commutation of leakage energy. In *Power Electronics, Machines and Drives (PEMD 2014), 7th IET International Conference on*, pages 1–5, April 2014.

[52] Hisashi Fujimoto, Kazuo Kuroki, T. Kagotani, and H. Kidoguchi. Photovoltaic inverter with a novel cycloconverter for interconnection to a utility line. In *Industry Applications Conference, 1995. Thirtieth IAS Annual Meeting, IAS '95., Conference Record of the 1995 IEEE*, volume 3, pages 2461–2467 vol.3, 1995.

[53] S. Nath and N. Mohan. A matrix converter fed sinusoidal input output three winding high frequency transformer with zero common mode voltage. In *Power Engineering, Energy and Electrical Drives (POWERENG), 2011 International Conference on*, pages 1–6, 2011.

[54] K.V. Iyer, K. Basu, W.P. Robbins, and N. Mohan. Determination of the optimal thickness for a multi-layer transformer winding. In *Energy Conversion Congress and Exposition (ECCE), 2013 IEEE*, pages 3738–3741, 2013.

[55] P.N. Enjeti, P.D. Ziogas, and J.F. Lindsay. Programmed pwm techniques to eliminate harmonics: a critical evaluation. *Industry Applications, IEEE Transactions on*, 26(2):302–316, 1990.

[56] Inductor datasheet. `http://www.coilws.com/images/ES55206-280M-160AH%20RevA-Web.pdf`.

[57] Capacitor datasheet. `http://capacitoredge.kemet.com/capedge2/DataSheet/Datasheet-C4BSNBX4100ZAFJ.pdf?pn=C4BSNBX4100ZAFJ`.

[58] M.P. Kazmierkowski, L.G. Franquelo, J. Rodriguez, M.A. Perez, and J.I. Leon. High-performance motor drives. *Industrial Electronics Magazine, IEEE*, 5(3):6–26, Sept 2011.

[59] E.G. Shivakumar, K. Gopakumar, S.K. Sinha, A. Pittet, and V.T. Ranganathan. Space vector pwm control of dual inverter fed open-end winding induction motor drive. In *Applied Power Electronics Conference and Exposition, 2001. APEC 2001. Sixteenth Annual IEEE*, volume 1, pages 399–405 vol.1, 2001.

[60] M.R. Baiju, K.K. Mohapatra, R.S. Kanchan, and K. Gopakumar. A dual two-level inverter scheme with common mode voltage elimination for an induction motor drive. *Power Electronics, IEEE Transactions on*, 19(3):794–805, May 2004.

[61] R. Baranwal, K. Basu, and N. Mohan. Carrier-based implementation of svpwm for dual two-level vsi and dual matrix converter with zero common-mode voltage. *Power Electronics, IEEE Transactions on*, 30(3):1471–1487, March 2015.

[62] R.K. Gupta, K.K. Mohapatra, A. Somani, and N. Mohan. Direct-matrix-converter-based drive for a three-phase open-end-winding ac machine with advanced features. *Industrial Electronics, IEEE Transactions on*, 57(12):4032–4042, Dec 2010.

[63] Saurabh Tewari, Ranjan K Gupta, Apurva Somani, Ned Mohan, and Life Fellow. Indirect Matrix Converter Based Open-End Winding AC Drives With Zero Common-Mode Voltage. pages 1520–1527, 2016.

[64] Saurabh Tewari, Ranjan Kumar Gupta, and Ned Mohan. Three-level indirect matrix converter based open-end winding AC machine drive. In *IECON 2011 - 37th Annual Conference of the IEEE Industrial Electronics Society*, number 1, pages 1636–1641. IEEE, nov 2011.

[65] S. Gandikota and N. Mohan. Single stage transformer isolated high frequency ac link based open end drive. In *2016 IEEE Applied Power Electronics Conference and Exposition (APEC)*, pages 1051–1056, March 2016.

[66] S. Chen, T. A. Lipo, and D. Fitzgerald. Source of induction motor bearing currents caused by PWM inverters. *IEEE Transactions on Energy Conversion*, 11(1):25–32, 1996.

[67] Fei Wang, A.K. Wallace, Shaoan Dai, Annette Von Jouanne, and Haoran Zhang. Multilevel inverter modulation schemes to eliminate common-mode voltages. *IEEE Transactions on Industry Applications*, 36(6):1645–1653, 2000.

[68] Satoshi Ogasawara, Hideki Ayano, and Hirofumi Akagi. An active circuit for cancellation of common-mode voltage generated by a PWM inverter. *IEEE Transactions on Power Electronics*, 13(5):835–841, 1998.

[69] M. R. Baiju, K. K. Mohapatra, R. S. Kanchan, and K. Gopakumar. A dual two-level inverter scheme with common mode voltage elimination for an induction motor drive. *IEEE Transactions on Power Electronics*, 19(3):794–805, 2004.

[70] E.G. Shivakumar, K Gopakumar, S.K. Sinha, A Pittet, and V.T. Ranganathan. Space vector PWM control of dual inverter fed open-end winding induction motor drive. In *APEC 2001. Sixteenth Annual IEEE Applied Power Electronics Conference and Exposition (Cat. No.01CH37181)*, volume 1, pages 399–405. IEEE, 2001.

[71] S. Gandikota and N. Mohan. A new leakage energy commutation technique for single stage high frequency link inverters. In *Power Electronics, Drives and Energy Systems (PEDES), 2014 IEEE International Conference on*, pages 1–6, Dec 2014.

[72] Chee-Lim Nge and Z. Salam. Application of natural commutation technique to center-tapped hf link inverter. In *Power Electronics and Drives Systems, 2005. PEDS 2005. International Conference on*, volume 1, pages 90–94, 2005.